



Abschlussarbeit im Bachelorstudiengang Physik

Untersuchung der Modellabhängigkeit der Partialwellenanalyse des Drei-Pionen-Endzustandes

Study of the model dependence of the partial-wave analysis of the
three-pion final state

Xuanyou Pan

30. July 2018

Erstgutachter (Themensteller): Prof. S. Paul
Zweitgutachter: Prof. R. Gross

Contents

1	Introduction	1
2	Fundamentals	3
2.1	The Process	3
2.2	Partial-Wave Formalism	3
2.3	Maximum Likelihood Method	7
2.4	Monte Carlo Method	8
3	Analysis for the Monte Carlo data	9
3.1	Preparation	9
3.2	Results and Discussion	14
4	Analysis for the Real Data	31
4.1	Preparation	31
4.2	Results and Discussion	33
5	Conclusions	39
6	Outlook	41
A	Isobar Parameterizations	43
B	Large Tables	45
	Bibliography	51
	Acknowledgements	53

Chapter 1

Introduction

Hadron spectroscopy is an important part of particle physics. It studies the masses and decays of hadrons. Quantum chromodynamics (QCD) is the theory of strong interaction that predicts these properties of hadron. QCD has been already confirmed by many experimental evidences. However, it cannot calculate the low energy scale, as the running coupling constant α_s impedes the convergence of its expansion, so that in principle an infinite number of Feynman diagrams have to be taken into account. In order to know more about the strong interaction in this special energy range, more experimental hints is required.

Light mesons are of particular interest because they belong to hadrons with low energy. They are quark-antiquark bound states of up, down or strange quarks. In 2008, an experiment was conducted at the COMPASS experiment at CERN, where a π^- beam with fixed energy of 190 GeV interacted with a stationary liquid-hydrogen target [1]. The proton recoiled and the π^- produced excited meson that decayed after the interaction. Among all the decay modes, the $\pi^- \pi^- \pi^+$ mode has the largest data set. The giant amount of data minimizes the statistical fluctuation so that we are more likely to extract convincing outcomes.

This thesis shows a study of the $\pi^- \pi^- \pi^+$ data based on a previous analysis model [2]. The goal of the thesis is to test the robustness of the model using the Monte Carlo data and to extract the isobar parameters from the experimental data by fitting them to the model. The second chapter explains the analysis method. The third chapter presents the analysis result for the Monte Carlo data to research the model. The fourth chapter applies the model to the real experimental data to extract parameters. The fifth chapter gives the conclusion and the sixth chapter a brief outlook.

Chapter 2

Fundamentals

2.1 The Process

The thesis studies the process

$$\pi^- + p \rightarrow \pi^- + \pi^- + \pi^+ + p_{\text{recoil}} \quad (2.1)$$

The data taken from the experiment contains the kinematic distribution of the final-state particles. For fixed target experiment with a monoenergetic incoming beam, the center-of-mass energy \sqrt{s} of the whole reaction is constant. The data consists of the 3π invariant mass $m_{3\pi}$, the four-momentum transfer squared t' , and a set of five additional phase-space variables denoted as τ that describes the 3π final state [2].

The goal of the analysis is to extract the 3π resonances and their quantum numbers from the data. To achieve this, a model was built for the analysis. The basic idea of the model construction is the partial-wave formalism.

2.2 Partial-Wave Formalism

In a narrow sense, partial-wave analysis (PWA) describes the expansion of the amplitude for elastic two-body scattering into spherical waves described by Legendre polynomials.¹ The spherical waves, well-defined by orbital angular momentum quantum numbers, are orthogonal to each other and build a complete basis, so that the amplitude can be fully decomposed and described. The concept can be extended to inelastic reactions such as the one shown in Eq. (2.1). Here, the daughter particles from the scattering can further decay into various particles. Hence the components of their partial waves can also be decomposed into more rudimentary component waves. The partial amplitude now represents the 3π system with well-defined quantum numbers.

¹See, for example, Eq.(6.4.29) in Ref. [3].

2.2.1 Analysis Model

Since resonance production and decay are independent, we can decompose the process in Eq. (2.1) into two independent parts: (i) the inelastic two-body scattering between the pion beam and the proton $\pi^- + p \rightarrow X^- + p_{\text{recoil}}$ and (ii) the subsequent decay of the resultant 3π resonance $X^- \rightarrow \pi^- + \pi^- + \pi^+$, as illustrated in figure 2.1.

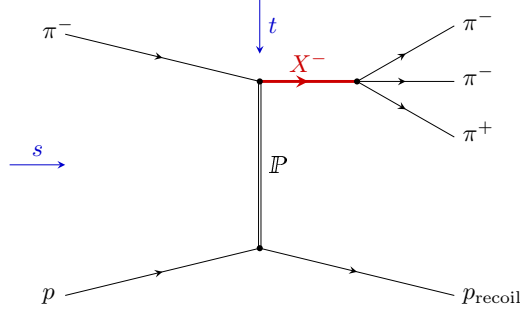


Figure 2.1: Diffractive dissociation of a beam pion into the three-pion final state on a target proton [2]

Mathematically, the matrix element for the process described in Fig. 2.1 can be factorized into two parts: a *transition amplitude* $\mathcal{T}(m_{3\pi}, t')$ for process (i) and a *decay amplitude* $\Psi(m_{3\pi}, \tau)$ for process (ii). The total intensity distribution is proportional to the squared matrix element, which is given by

$$\mathcal{I}(m_{3\pi}, t', \tau) \propto |\mathcal{M}(m_{3\pi}, t', \tau)|^2 = \left| \sum_i^{N_{\text{waves}}} \mathcal{T}_i(m_{3\pi}, t') \Psi_i(m_{3\pi}, \tau) \right|^2 \quad (2.2)$$

Here, the index i enumerates all the possible X^- and their decay modes. Each i can be defined via a specific set of quantum numbers:²

$$i \equiv \{I^G J^{PC} M; \xi, L\} \quad (2.3)$$

with I the isospin, J the total spin, M the spin projection, G the G-parity, P the parity and C the C-parity of resonance X . ξ and L contain the information of the further decays that will be explained in section 2.2.2.

According to our previous definition, the decay amplitude $\Psi_i(m_{3\pi}, \tau)$ labeled by index i corresponds to the partial wave, whose dependence on the kinematic variable can be calculated using *isobar model* that will be discussed in section 2.2.2.

²Here, the number of free parameters can be reduced using conservation laws. Details will be discussed in section 3.1.2

The transition amplitudes \mathcal{T}_i and their dependence on $m_{3\pi}$ and t' are unknown to us. However, the assumption that $\mathcal{T}_i(m_{3\pi}, t')$ is constant in narrow $(m_{3\pi}, t')$ cells enables us to group the experimental data in these cells, and get the values of $\mathcal{T} = (\mathcal{T}_1, \dots, \mathcal{T}_{N_{\text{waves}}})$ in each cell independently. We attain this goal by fitting Eq. (2.2) to the data. In this first stage of analysis, the τ -dependence of data is exploited and we simplify our 7-dimensional data analysis into a 2-dimensional. In the next stage, model will be constructed to study \mathcal{T} dependent on $m_{3\pi}$ and t' for our final goal. This thesis focus on the first stage.

2.2.2 Isobar Model

The decay amplitudes $\Psi_i(m_{3\pi}, \tau)$ are calculated using the *isobar model*. In this model, the decay $X \rightarrow 3\pi$ is described as a chain of successive two-body decays via intermediate resonances called *isobars* [4, 5]. This process is shown in figure 2.2.

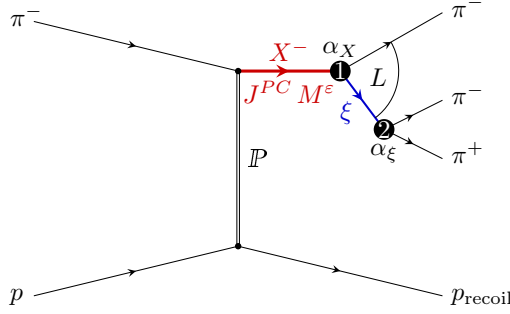


Figure 2.2: The decay of X^- via an intermediate resonance ξ as described in the isobar model [2]

The isobar model neglects the final-state interactions of the outgoing particles. Hence, each three-body decay amplitude $\Psi(m_{3\pi}, \tau)$ can be factorized into two-body decay amplitudes: (i) $\mathcal{A}_M^X(\theta_X, \varphi_X, m_{3\pi})$ for $X^- \rightarrow \xi^0 + \pi^-$ and (ii) $\mathcal{A}_\lambda^\xi(\theta_\xi, \varphi_\xi, m_{\pi\pi})$ for $\xi^0 \rightarrow \pi^- + \pi^+$. θ and φ represent the polar and azimuthal angles of one of the daughter particles in the respective two-body decay. M is the spin projection of X and λ is the helicity of the isobar ξ . Because the helicity is the intrinsic variable inside the decay chain and thus independent of the extrinsic three-body decay, all possible values of λ have to be summed over:

$$\Psi(\underbrace{\theta_X, \varphi_X, m_{\pi\pi}}_{\tau}, \theta_\xi, \varphi_\xi; m_{3\pi}) = \mathcal{A}_M^X(\theta_X, \varphi_X, m_{3\pi}) \sum_{\lambda} \mathcal{A}_\lambda^\xi(\theta_\xi, \varphi_\xi, m_{\pi\pi}) \quad (2.4)$$

Lets now focus on the two-body decay amplitude. The decay happens in a central potential, which allows the amplitude to be factorized into a *dynamic part* that only

depends on the masses of the parent and daughter particles, and an *angular part* that only depends on the polar and azimuthal angles. The two-body decay amplitude of ξ is given by

$$\begin{aligned} \mathcal{A}_{J_\xi M_\xi L_\xi S_\xi}^\xi(\theta_\xi, \varphi_\xi, m_{\pi\pi}) &\propto \underbrace{\alpha_{\xi \rightarrow \pi^+ \pi^-} F_{L_\xi}(m_{\pi\pi}) \Delta_\xi(m_{\pi\pi})}_{\text{dynamic part}} \\ &\cdot \sum_{\lambda_1, \lambda_2} \underbrace{(J_1, \lambda_1; J_2, -\lambda_2 | S_\xi, \lambda_1 - \lambda_2)(L_\xi, 0; S_\xi, \lambda_1 - \lambda_2 | J_\xi, \lambda_\xi) D_{M_\xi \lambda_\xi}^{J_\xi^*}(\theta_\xi, \varphi_\xi, 0)}_{\text{angular part}} \end{aligned} \quad (2.5)$$

Here, the *dynamic part* comprises a coupling term $\alpha_{\xi \rightarrow \pi^+ \pi^-}$, an angular-momentum barrier factor $F_{L_\xi}(m_{\pi\pi})$ and a propagator term $\Delta_\xi(m_{\pi\pi})$. The propagator term is parameterized using relativistic Breit-Wigner amplitudes of the form³

$$\Delta_\xi^{\text{BW}}(m_{\pi\pi}; m_0, \Gamma_0) = \frac{m_0 \Gamma_0}{m_0^2 - m_{\pi\pi}^2 - im_0 \Gamma(m_{\pi\pi})} \quad (2.6)$$

where m_0 and Γ_0 are the nominal mass and width of the resonance. Under the assumption of a single two-body decay channel, the mass-dependent width $\Gamma(m_{\pi\pi})$ is given by:

$$\Gamma(m_{\pi\pi}) = \Gamma_0 \frac{m_0}{m_{\pi\pi}} \frac{q}{q_0} \frac{F_{L_\xi}^2(q)}{F_{L_\xi}^2(q_0)} \quad (2.7)$$

with $q(m_{\pi\pi})$ the momentum of the π^\pm in the rest frame of the isobar. At the nominal resonance mass, the breakup momentum is given by $q_0 = q(m_0)$.

An issue of the analysis model is that the resonance parameters of the isobars, for example m_0 and Γ_0 , have to be taken from other experiments [6]. Depending on how well the resonance parameters are known, this may introduce uncontrollable model dependence in the analysis. The goal of this thesis is to study this model dependence in detail.

Furthermore, We assume that the coupling term $\alpha_{\xi \rightarrow \pi^+ \pi^-}$ is independent of $m_{\pi\pi}$. The barrier factor $F_L(m_{\pi\pi})$, also appears in Eq.(2.7), takes into account the barrier effect caused by the orbital angular momentum L in the two-body decay.⁴

According to the helicity formalism [8], the *angular part*, representing the angular distribution of a given resonance ξ , can be described using orthogonal Wigner D -functions [9] with Clebsch-Gordan coefficients. The Wigner D -functions are labeled

³For some resonances, like $f_0(980)$ and $f_0(500)$, other parametrizations have to be applied. Details can be found in Ref. [2].

⁴The parametrization of von Hippel and Quigg was applied [7]. Detailed example of the expression for low L can be found in Ref. [2].

by the specific spin state $|J, M\rangle$ of the resonance. Since the $|J, M\rangle$ basis is complete, the angular part can thus be expressed as a linear combination of these basis states.

Till here, we found the decay amplitudes as known functions defined by isobar parameters, so that our model can be fitted to the data.

2.3 Maximum Likelihood Method

To determine the best parameter set for a given model from a data set, fit methods are adopted. Among them, the least-squares method and maximum likelihood method are generally used. The least-squares method is impractical for in high-dimensional fits (in our case five-dimensional), since the data must be subdivided into bins and the number of bins will increase exponentially with the growth of dimension. So here, we use the *maximum likelihood method*, where a *likelihood function* dependent on parameter set and data set will be maximized.

2.3.1 Likelihood Function

A likelihood function is defined as the joint probability density of the data set given the parameter values [10]. Given a data set $\mathbf{x} = (x_1, \dots, x_N)$ of N independent identical distributed random variables with the same probability density function $f(x; \boldsymbol{\theta})$ that depends on m parameters $\boldsymbol{\theta} = (\theta_1, \dots, \theta_m)$, the likelihood function is

$$\mathcal{L}(\boldsymbol{\theta}; \mathbf{x}) = \prod_{n=1}^N f(x_n; \boldsymbol{\theta}) \quad (2.8)$$

The maximum likelihood estimate $\hat{\boldsymbol{\theta}}$ for the parameters is given by

$$\hat{\boldsymbol{\theta}} = \arg \max_{\boldsymbol{\theta}} \mathcal{L}(\boldsymbol{\theta}; \mathbf{x}) \quad (2.9)$$

Here, \mathcal{L} is the probability density of the *data* instead of the parameters. Thus, \mathcal{L} is usually not normalized with respect to the parameters. Moreover, in a strictly mathematical sense, the maximization of the likelihood function under observed data does not necessarily yield the most probable parameter values.

2.3.2 Application

In the intensity distribution in Eq.(2.2), we regard the transition amplitudes $\mathcal{T} = \{\mathcal{T}_i\}$ as the free fit parameter set and the 5-dimensional phase-space variables τ as the random variables. The likelihood function for our model is then defined as [2]

$$\mathcal{L}(\mathcal{T}; \{\tau_n | n \in \{1, 2, \dots, N\}\}) = \underbrace{\frac{\bar{N}^N}{N!} \exp(-\bar{N})}_{\text{Poisson probability}} \prod_{n=1}^N \underbrace{\frac{\mathcal{I}(\tau_n)}{\int d\phi_3(\tau) \eta(\tau) \mathcal{I}(\tau)}}_{\text{Probability for event } i} \quad (2.10)$$

Here, N is the number of events we measured with phase space coordinates τ_n respectively. $\eta(\tau)$ is the detector efficiency, $d\phi_3(\tau)$ the differential three-body phase-space element, and $\bar{N} = \int d\phi_3(\tau) \eta(\tau) \mathcal{I}(\tau)$ the expected number of events in the detector.⁵ In addition, a Poisson probability density is multiplied as the model for counting experiments with events produced randomly with constant timely-averaged rates. The model parameter \bar{N} represents the expected number of events.

Exploiting the monotonicity of the logarithmic function, one often adopts the logarithm of the likelihood function to convert the product to a sum and to make the function numerically more stable. By maximizing the $\log \mathcal{L}$ function, one obtains a fit result, which consists of the most possible set of the transition amplitudes \mathcal{T} and its the $\log \mathcal{L}$ value.

2.4 Monte Carlo Method

Monte Carlo methods are a broad class of computational algorithms that rely on repeated random sampling to obtain numerical results. They are useful when it is difficult or impossible to use other approaches.

Specific for our process, we perform an analysis of pseudo data (also called Monte Carlo data) generated from a fitted model to the real data with this method. Using the Monte Carlo data, the properties of the model can be rightly studied. This is because in case we use the real data for study the model, the mismatching between the data and the model can influence the fit results, so that we cannot ascribe the deviations to the model itself.

Technically, we first generate uniformly distributed data in the 5-dimensional phase space. The generated data are then deweighted using a so-called *acceptance-rejection method* [11]. That is, the intensities are calculated using Eq. (2.2) for all uniform distributed data points. To make the intensity distributed uniformly, we generate a random number between zero and the maximal intensity and compare the calculated intensity value with this random number. If the calculated intensity is smaller than the this number, we keep the data point. If it is larger, we discard it. In this way, the remained data points distribute under our given model.

⁵The detector efficiency will be set to 1 for all phase space components for the Monte Carlo data.

Chapter 3

Analysis for the Monte Carlo data

In this chapter, I study the influence of the isobar parameters variation on the fit results using the Monte Carlo data. The data was generated according to the PWA result from Ref. [2] with two different 3π mass bins, $m_{3\pi} = 1.8 \text{ GeV}$ and $m_{3\pi} = 1.0 \text{ GeV}$. I test the stability of the fit results by fitting this data to the model where the isobar parameters are systematically shifted. Considering the discussion in section 2.3, a fit result is represented by the set of the transition amplitudes that gives the largest $\log \mathcal{L}$ value. Accordingly, the following analysis will focus on these two factor: the shift of transition amplitudes and the $\log \mathcal{L}$ values under variation of isobar parameters.

3.1 Preparation

3.1.1 Model Parameters

Empirically, the analysis model takes six different isobars into account: $[\pi\pi]_S$, $\rho(770)$, $f_0(980)$, $f_2(1270)$, $f_0(1500)$ and $\rho_3(1690)$.¹ Among them, the parameter dependence of $\rho(770)$, $f_2(1270)$, $f_0(1500)$ and $\rho_3(1690)$ will be studied. All these 4 isobars use Breit-Wigner parameterizations with slight modifications concerning their individual properties. Their parameters are shown in table 3.1 . The exact formulas of the parameterization can be found in Appendix A.

isobar	mass m_0 (MeV)	width Γ_0 (MeV)
$\rho(770)$	769.0	150.9
$f_2(1270)$	1275.1	185.1
$f_0(1500)$	1505.0	109.0
$\rho_3(1690)$	1688.8	161.0

Table 3.1: Overview of the PDG parameters of the resonances studied in this thesis [6]

¹Here, $[\pi\pi]_S$ represents a special parameterization that is not Breit-Wigner like and includes the broad $f_0(500)$ resonance. A comprehensive description of all these isobars can be found in Ref. [2].

3.1.2 The partial waves

According to section 2.2.1, each transition amplitude is labeled by the index i , which, according to Eq. (2.3), is determined by the intermediate state X^- and its quantum numbers. The model takes into account the isobars mentioned in section 3.1.1 with the spin $J \leq 6$ and $L_{\xi\pi} \leq 6$ for the subsequent π -isobar system. The PWA model consists of 88 partial waves in total. The complete list of waves is found in Appendix B.

There, for each partial wave, the characteristic quantum numbers can be concluded via $[I^G, J^P, M^\varepsilon] \rightarrow \{\text{Isobar } \xi \rightarrow \{\pi^- [L_{2\pi}, S_{2\pi}] \pi^+\} [L_{\xi\pi}, S_{\xi\pi}] \pi^-\}$ with the quantum numbers described in Eq. (2.3). The L and S are the orbital angular momentum and the spin in each subsystem. Some of these quantum numbers are redundant due to the resonance properties and the conservation laws. Firstly, the isospin I is determined by the constituents of the system. For the 3π resonance $I = 1$. In this way, the isospin I and the G-Parity G can be concluded into C-Parity C with $G = C(-1)^I$. In addition, pion is a spin-0 particle, which means that the spin $S_{2\pi} = 0$ for all partial waves. For the same reason, the orbital angular momentum $L_{2\pi}$ and the total spin $S_{\xi\pi}$ are equal to the spin of ξ for all the partial waves. Taken these constraints into consideration, the description of the partial wave is reduced to the form $J^{PC} M^\varepsilon \xi L_{\xi\pi}$.

For each 3π invariant mass, we fit the model with the 88 partial waves to the data. However, for a low $m_{3\pi}$, the fit result can be instable. This is because the range for $m_{\pi\pi}$ for a low $m_{3\pi}$ is limited by phase space, so that some partial waves become indistinguishable and the $\log \mathcal{L}$ becomes in effect multimodal. The problem can be solved adding threshold values for specific partial waves (See App. B). For $m_{3\pi}$ below the threshold value, the partial wave will not be taken into account and its intensity will be set to zero.

3.1.3 Fit for the right parameters

The generic minimization algorithms make it easier to minimize a given function than to maximize. Therefore, to study the modalities of the $-\log \mathcal{L}$ function, I performed the PWA fit for about a thousand random start values and plotted the resultant transition amplitudes distribution. The outcomes are shown as follows.

$m_{3\pi} = 1.8 \text{ GeV}$

For the Monte Carlo data from the best fit result of the real experimental data with $m_{3\pi} = 1.8 \text{ GeV}$, Fig. 3.1a shows the results of a single partial wave as an ex-

ample. Here, I was not sure whether the cloud of points represents a single minimum with numerical deviation from the computational algorithm, or a fluctuation of the function itself. I solved the problem by adding a relative scale to the figure: For data sets with a large number of events, the \mathcal{L} function is approximately normal distributed in terms of the parameters. The $-\log \mathcal{L}$ function should then be parabolic and the parameter resolution can be estimated. Under the Gaussian assumption, a 0.5 unit elevation of $-\log \mathcal{L}$ corresponds to 1σ range of the parameter. Marking this range of the best fit result with the lowest $-\log \mathcal{L}$ value, I got an uncertainty ellipse presented in Fig. 3.1b. Adding this gauge to the figure, it is now more convincing that the $-\log \mathcal{L}$ function has a single global minimum.

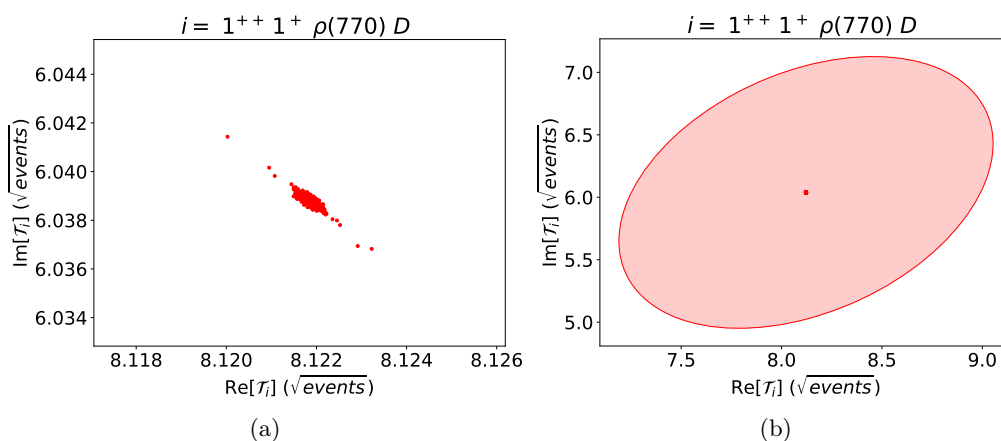


Figure 3.1: Panel (a) shows the fit results distributed in the transition amplitude of a partial wave for the Monte Carlo data with $m_{3\pi} = 1.8 \text{ GeV}$. Panel (b) shows the results and the uncertainty ellipse of the best result.

I also gave some evidence for the Gaussian assumption. Provided that the assumption be true, the $-\log \mathcal{L}$ would be parabolic distributed. So $-\log \mathcal{L}$ dependent on real or imaginary part of each transition amplitude can be fitted parabolic. To confirm that, I calculated the $-\log \mathcal{L}$ functions along the transition amplitudes, plotted the distribution and fitted them parabolic. Fig. 3.2a shows the the outcome for the same partial wave as Fig. 3.1a. Here, up to a raise of about 0.5 unit of $-\log \mathcal{L}$, the transition amplitude distributed perfectly parabolic. The assumption is positively supported.

In addition, the disagreement of the parable and the data point can be quantified by the sum of the squared differences between them, $\sum_i \delta_i^2$. A small $\sum_i \delta_i^2$ value

means a good fit. Consequently, a parabolic fit with a larger $\sum_i \delta_i^2$ indicate that the data is not thoroughly parabolic. In this case, the Gaussian assumption is no more justified. For example, Fig. 3.2b shows the fit with the largest $\sum_i \delta_i^2$. Here, the two curves overlap no more.

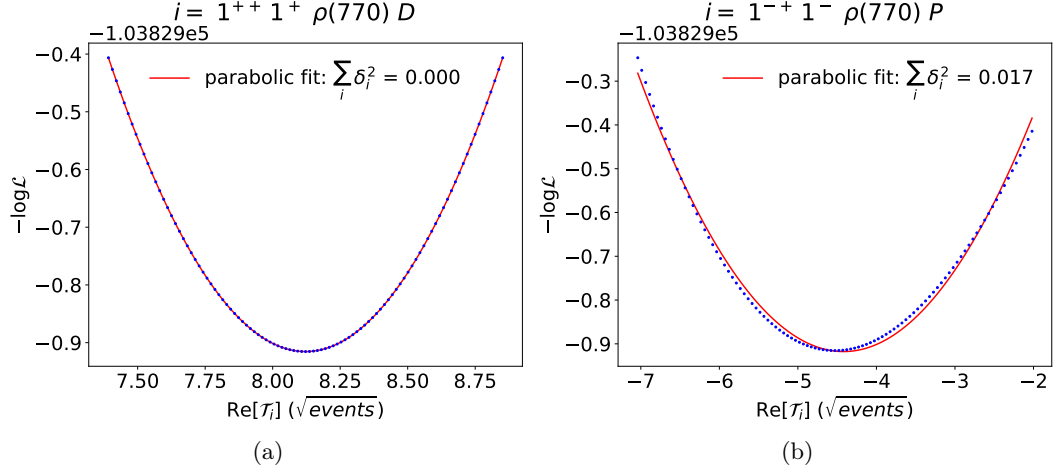


Figure 3.2: Panel (a) and (b) show the $-\log \mathcal{L}$ function along the real part or the imaginary part of one transition amplitude and its parabolic fit.

The Gaussian assumption is important to the uncertainty estimation. I calculated for each partial wave equidistant 100 points along its transition amplitude with the $-\log \mathcal{L}$ between its lowest value and 0.5 unit above to get comparable $\sum_i \delta_i^2$ for each wave. Table 3.2 gives a list of the parameters with $\sum_i \delta_i^2$ greater than 0.01.

Partial wave	Part	$\sum_i \delta_i^2$
$1^{-+} 1^- \rho(770) P$	real	0.0173
$2^{++} 0^- \rho(770) D$	imaginary	0.0149
$2^{-+} 1^- f_2(1270) S$	real	0.0148
$2^{++} 0^- \rho(770) D$	real	0.0110

Table 3.2: Transition amplitudes with a relative large deviation from the gaussian assumption

$m_{3\pi} = 1.0 \text{ GeV}$

I generated Monte Carlo data from the best fit result with threshold for

$m_{3\pi} = 1.0 \text{ GeV}$. As the Monte Carlo data can be perfectly described by the model, the fit result should be more stable. Here, it would be particularly interesting to study the impact of the thresholds. Thus, I fitted the model without threshold to the data at first and examined its stability.

I used the same analysis method. Fig. 3.3a shows the fit results distribution. Here unfortunately, the $-\log \mathcal{L}$ function is still multimodal. Yet, These local minimums have different $-\log \mathcal{L}$ values. As discussed in the former section, domain up to 0.5-unit elevation in the $-\log \mathcal{L}$ represents an area of uncertainty. The statement can be extended: one only needs to focus on the local minimums in this range. Adding this constraint, I plotted the distribution of the fit results without the irrelevant points. It is shown in Fig. 3.3b with a single global minimum. There are no other comparable results to the best fit result. This is extremely favorable to us as it simplifies the analysis drastically. Moreover, there are 722 from the total 1004 fit results plotted in Fig. 3.3b. This means that 1000 fit attempts are sufficient to find the global minimum.

Considering the above analysis, I will only take the fit results with $-\log \mathcal{L}$ lower than the 0.5 elevation upon the best fit result into consideration for the further analysis.

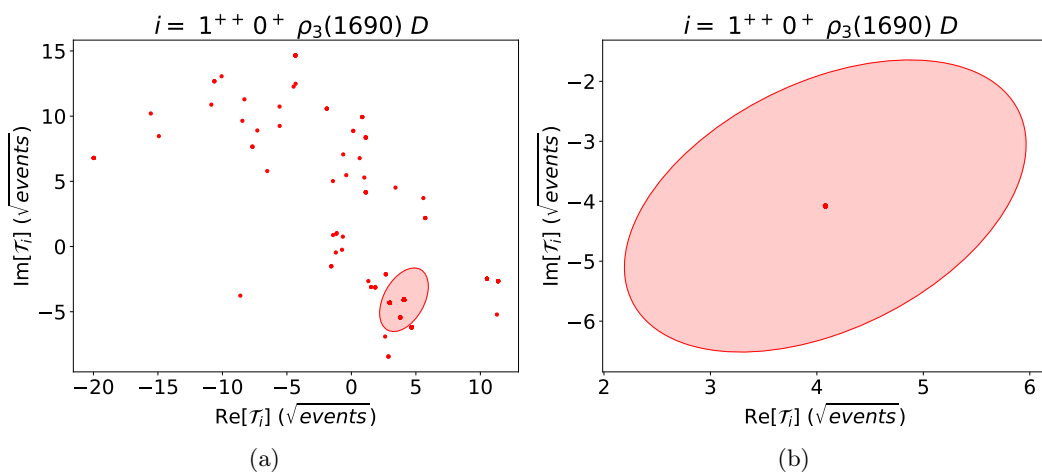


Figure 3.3: Panel (a) shows all fit results distributed in the transition amplitude of a partial wave for the Monte Carlo data with $m_{3\pi} = 1.0 \text{ GeV}$ and the uncertainty ellipse of the best fit result. Panel (b) shows the fit results with their $-\log \mathcal{L}$ value within 0.5-unit elevation of the best fit result.

The Effect of Thresholds

The thresholds ensure the fit stability for the data with low $m_{3\pi}$. It would be interesting to compare the fitted transition amplitudes for model with and without threshold. As demonstrated in section 2.2.2, the angular part of the decay amplitudes depends uniquely on the sort of the isobar and its quantum numbers. Hence, among the partial waves with different decay mode, those with the same set of quantum numbers may interfere to a higher degree. For example, the partial waves $0^{-+}0^{+} [\pi\pi]_S S$, $0^{-+}0^{+} f_0(980) S$ and $0^{-+}0^{+} f_0(1500) S$ have the same quantum numbers. The latter two are thresholded at $m_{3\pi} = 1.0 \text{ GeV}$. Thus, I compared the fit results of these three waves with and without thresholds.

As shown in Fig. 3.4a, 3.4c and 3.4e, the fit results for Monte Carlo data with $m_{3\pi} = 1.0 \text{ GeV}$ are compatible with and without threshold. That is, for thresholded waves, the fit without threshold gives small transition amplitudes and the ‘zero’s are contained in the uncertainty ellipses; for the non-thresholded wave, the uncertainty ellipses of the both best fit results overlap. However, concerning the real data at the same 3π invariant mass shown in Fig. 3.4b, 3.4d and 3.4f, the fit results are no more in consistence.

In conclusion, if the data is distributed strictly according to a given model, the fit algorithm has no problem distinguishing the similar waves. On the contrary, in case of the real data, one is not sure about the exact constituents of the partial wave. This slight ambiguity leads to the systematic uncertainty of fit results and in effect a high sensibility of the model.

3.2 Results and Discussion

In this section, I study the shift of the transition amplitudes and the $-\log \mathcal{L}_{\text{best}}$, $-\log \mathcal{L}$ of the best fit results dependent of the isobar parameters. The study uses the same Monte Carlo data as the section 3.1.3 and bases on the PWA model used for real data. I changed the isobar parameters individually for up to $\pm 10 \text{ MeV}$ relative to the values in table 3.1, corresponding approximately to the mass resolution, and kept the other isobar parameter unchanged. For each set of the isobar parameters inputted to the model, I performed the PWA fit for about a thousand time using random start values for the transition amplitudes. These fit results will be studied as follows.

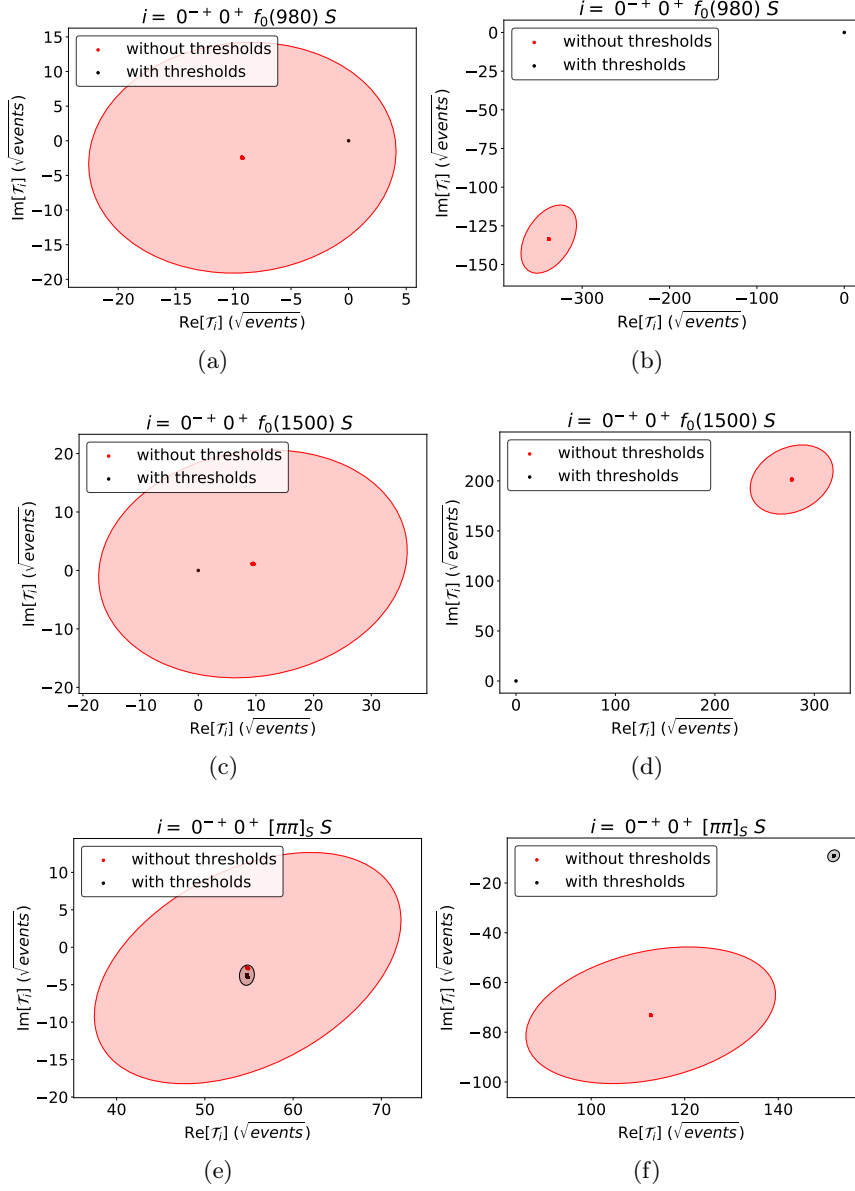


Figure 3.4: Panel (a), (c) and (e) show the fit results distributed in the transition amplitude for the Monte Carlo data with $m_{3\pi} = 1.0$ GeV and the uncertainty ellipses. Panel (b), (d) and (f) show the fit results for the real data with $m_{3\pi} = 1.0$ GeV.

3.2.1 Shift of Transition Amplitudes

To visualize the fit results, I plotted the distribution of the transition amplitudes from the 1000 fit attempts. As discussed in section 3.1.3, only the fit results with $-\log \mathcal{L} < -\log \mathcal{L}_{\text{best}} + 0.5$ were taken into account. To distinguish the isobar parameter values, different colors are used. Fig. 3.5 shows some examples of the resultant plots. Here, all fit attempts converged to the same solution. Actually, all plots have this property. This means that the $-\log \mathcal{L}$ functions have a well-defined minimum for all the isobar parameters. Consequently, the fit is stable and the PWA model is robust w.r.t. changes of these isobar parameters.

According to Fig. 3.5, the fit has different susceptibility to the changes of isobar parameters. To analyze the differences, one needs to compare the plots. Yet, the analysis task is multidimensional. That is, the plots are defined by (i) data from two different 3π invariant masses, (ii) variation in terms of each isobar parameter and (iii) the results of all transition amplitudes. I will discuss the points respectively as follows.

A. $m_{3\pi}$ dependence

According to Fig. 3.5a and 3.5b concerning the isobar parameters $m_{0,\rho(770)}$ and $m_{0,f_0(1500)}$ for $m_{3\pi} = 1.8 \text{ GeV}$, evident shifts of the fit results can be observed for both cases. In comparison, for the data with $m_{3\pi} = 1.0 \text{ GeV}$, the fit results is still susceptible to changes of $m_{0,\rho(770)}$ (Fig. 3.5c), while the transition amplitude is independent of $m_{0,f_0(1500)}$ (Fig. 3.5d). In fact, the data with $m_{3\pi} = 1.0 \text{ GeV}$ is only susceptible to the changes of $\rho(770)$ parameters. For the data with $m_{3\pi} = 1.8 \text{ GeV}$, recognizable shifts can be observed at changes of all the isobar parameters.² The possible reason for that is presented as follows.

According to section 2.2.2, the isobar parameters affect merely the propagator term in the dynamic part of the decay amplitudes. Among all the isobars, the $f_0(1500)$ has a relative simple parameterization, as its width can be regarded as a constant (Eq. (A.2)). I use this parameterization as an example to get a rough perception. Fig. 3.6a shows the parameterization.

Due to the energy conservation, the $m_{\pi\pi}$ range for a fixed 3π invariant mass is limited. The maximum $m_{\pi\pi}$ value cannot exceed $(m_{3\pi} - m_\pi)$. Explicitly for the two $m_{3\pi}$ values of our data, the $m_{\pi\pi}$ ranges are marked in Fig. 3.6a. For the $f_0(1500)$, the

²For $\rho_3(1690)$, the fit results shifts weaker even for $m_{3\pi} = 1.8 \text{ GeV}$. That can be refer to the fact that only part of the peak of the propagator term is kinematically accessible for this 3π mass (Fig. 3.6b). See the discussion as follows.

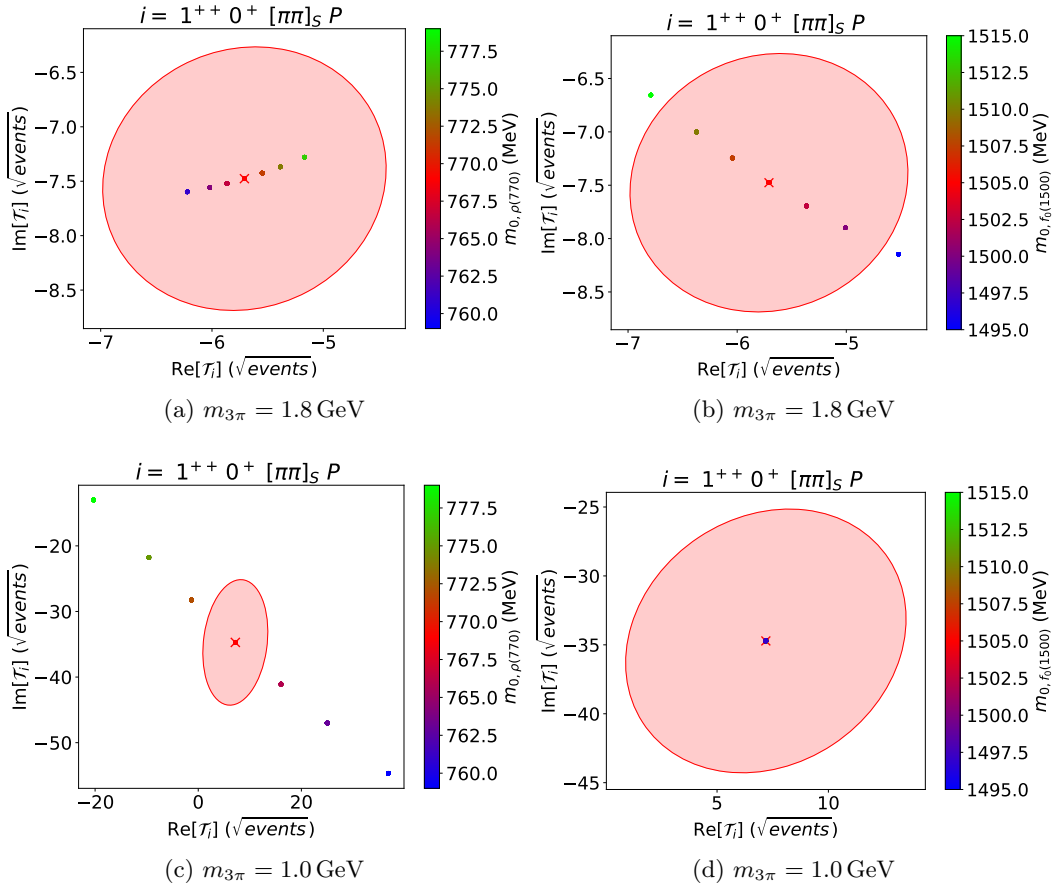


Figure 3.5: The figures show the transition amplitudes from PWA fit to the Monte Carlo data for different values of isobar parameters represented by the color bars. The best fit result of the isobar parameters in table 3.1 is marked by the red cross and its uncertainty ellipse is shown.

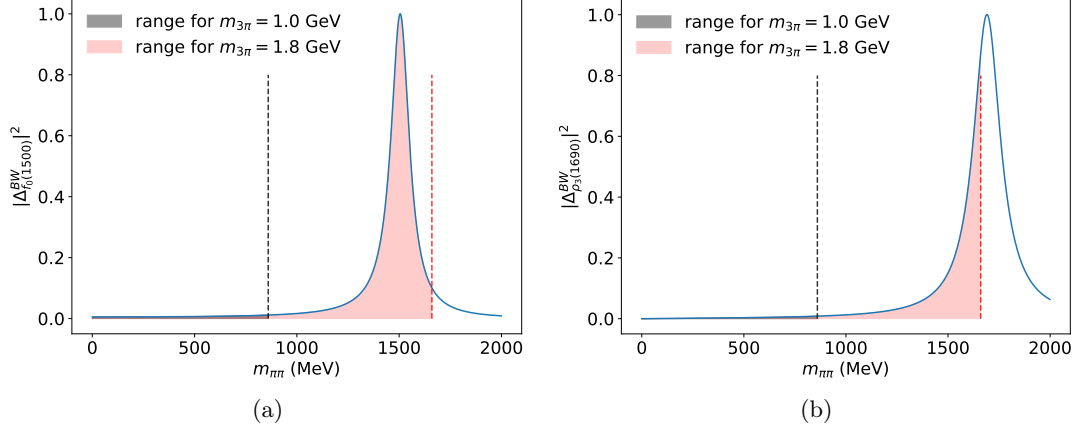


Figure 3.6: Breit-Wigner parameterization for the propagator term of (a) the $f_0(1500)$ and (b) the $\rho_3(1690)$

kinematically accessible area for data with $m_{3\pi} = 1.0$ GeV is limited to the low-mass tail of the $f_0(1500)$. The $f_0(1500)$ peak is apparently outside this range so that a shift or deformation of this peak can hardly influence the shape in the accessible $m_{\pi\pi}$ range. As a result, the fit result should be insensitive to changes of isobar parameters with $m_{0,\xi} > m_{3\pi}$ of the data. This has been positively proved by the outcomes, for example, Fig. 3.5.

B. Comparison between changes of mass and width

Another interesting aspect is the comparison between the influence of mass and width changes of each isobar on transition amplitudes. Simple examples are in Fig. 3.7, where the transition amplitudes from PWA fit w.r.t. changes of $f_0(1500)$ parameters for data with $m_{3\pi} = 1.8$ GeV, and changes of $\rho(770)$ parameters for data with $m_{3\pi} = 1.0$ GeV are shown. Here, the fits are more susceptible to the masses changes than the widths changes concerning one changed isobar. The possible reason is given as follows.

Again, I take the parameterizations of $f_0(1500)$ as an example. According to Fig. 3.8, a change in $m_{0,f_0(1500)}$ will shift the position of the peak and a change in $\Gamma_{0,f_0(1500)}$ will alter the width of the peak. Focusing on the function values of each points, one finds that a change of the peak position steer the intensity distribution greater than the width, as it affects all the points near both the previous peak and the shifted. As a result, we found the shift of the transition amplitudes are more susceptible to

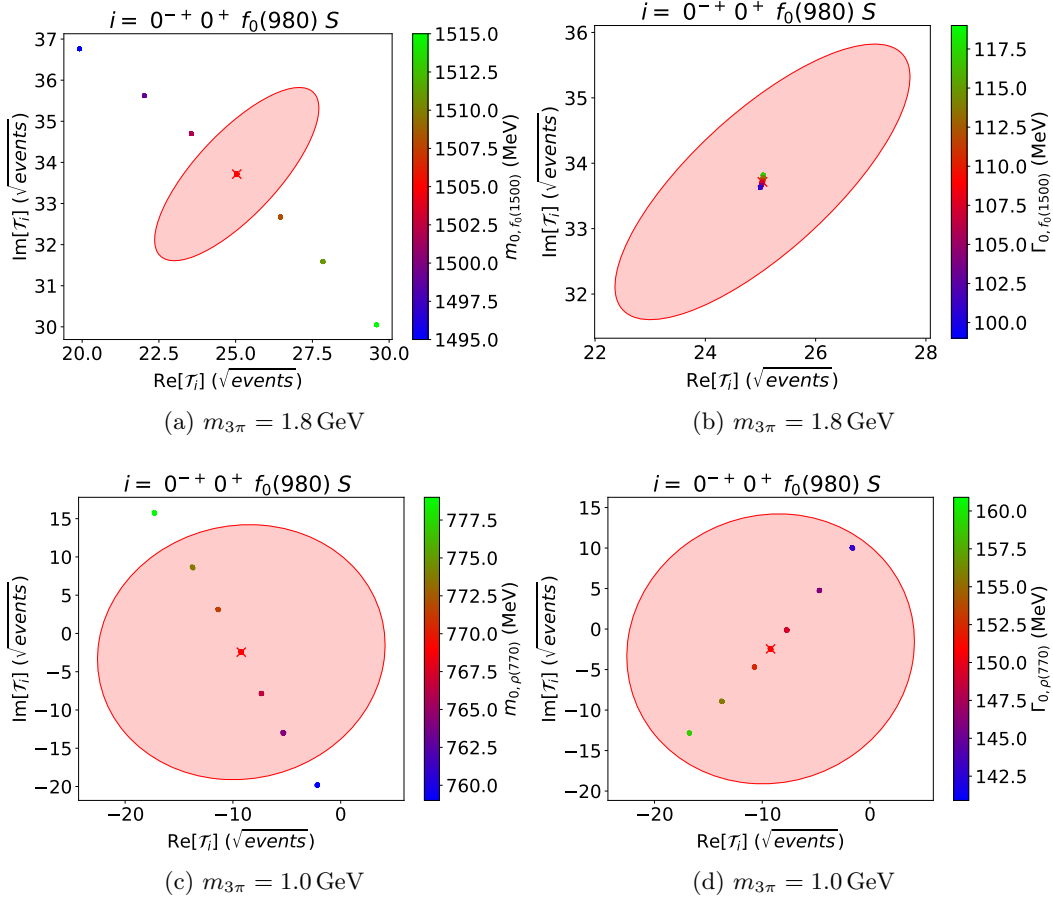


Figure 3.7: The figures show the transition amplitudes from PWA fit to the Monte Carlo data for different values of isobar parameters represented by the color bars. The best fit result of the isobar parameters in table 3.1 is marked by the red cross and its uncertainty ellipse is shown.

the isobar masses changes than its widths for data with the same $m_{3\pi}$.

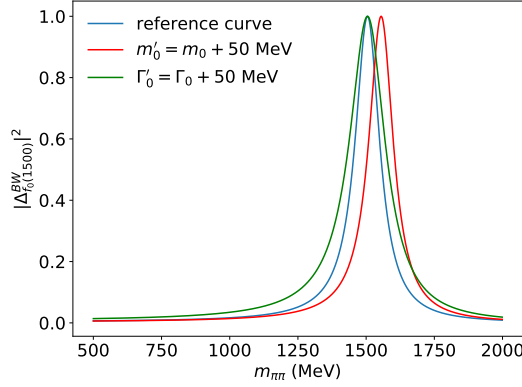


Figure 3.8: Breit-Wigner parameterizations for the propagator term of $f_0(1500)$. The reference curve (blue) uses the parameters in table 3.1, while the other two curves (red and green) are with the change of one parameter from them.

A slight exception can be predicted for the parameter changes of $\rho_3(1690)$. According to Fig. 3.6b, even for the fit to the data with $m_{3\pi} = 1.8$ GeV, the peak is only partly kinematically accessible. In this case, changes of the both parameters should affect the fits to a similar degree. Fig. 3.9 proved the prediction. The same effect appears concerning the changes of parameters of $\rho(770)$ to the Monte Carlo data with $m_{3\pi} = 1.0$ GeV: the disparity between Fig. 3.7c and 3.7d is smaller than between Fig. 3.7a and 3.7b.

The above analysis brings me to a summary: how far the fit results shift is closely interrelated with the scale of the deviation in the parameterization function from the origin values. Quantitatively, the changes of the isobar masses are $(m_0 \pm 3)$, $(m_0 \pm 6)$ and $(m_0 \pm 10)$ MeV/ c^2 ; the changes of its widths are $(\Gamma_0 \pm 2)$, $(\Gamma_0 \pm 6)$ and $(\Gamma_0 \pm 10)$ MeV/ c^2 . From, for example, Fig. 3.7c, 3.7d, 3.9a and 3.9b, I summarize the properties:

- 1) The fit results under changes of each single parameter build up roughly a line on the complex plain of each transition amplitude.
- 2) The shift degree of the transition amplitudes is roughly linear to the shift degree of the isobar parameter.

These properties reduce the information from the plots greatly. As we only focus on the how much the transition amplitudes shift compared to the range of the statistical

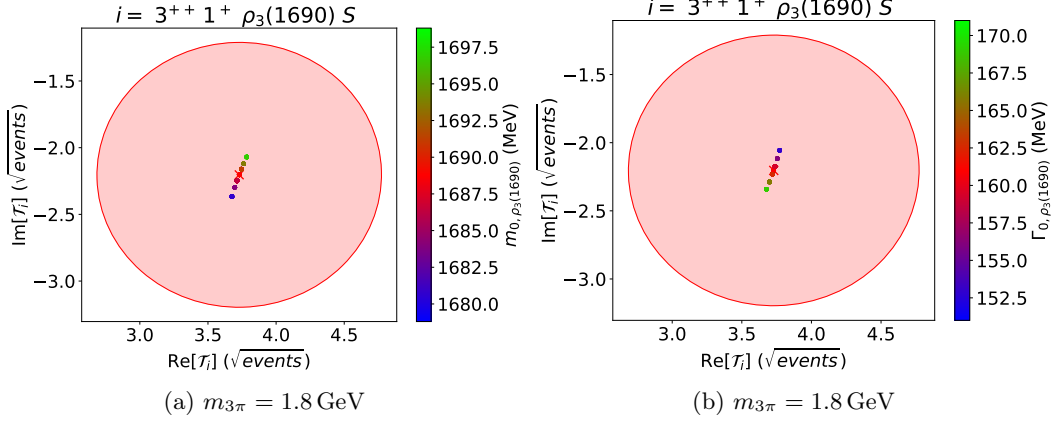


Figure 3.9: The figures show the transition amplitudes from PWA fit to the Monte Carlo data for different values of $\rho_3(1690)$ parameters represented by the color bars. The best fit result of the isobar parameters in table 3.1 is marked by the red cross and its uncertainty ellipse is shown.

uncertainty, it is sufficient to compare the extension of the largest shifts w.r.t. isobar parameter's changes with the scope of the uncertainty ellipse in the same direction. Mathematically, we define a measure Δ for how strongly a transition amplitude depends on the isobar parameter with

$$\Delta = \frac{1}{2} \cdot \left(\frac{d_1}{R_1} + \frac{d_2}{R_2} \right) \quad (3.1)$$

with R_1 , R_2 , d_1 and d_2 shown in Fig. 3.10.

C. Comparison among the partial waves

Table 3.3 shows the Δ calculated from Eq. 3.1 for $m_{3\pi} = 1.8 \text{ GeV}$. To facilitate the analysis, I grouped the values by columns concerning different change of isobar parameter. The row blocks gather the entries with the same quantum numbers J^{PC} . Moreover, the entries larger than 1, corresponding to a shift outside the uncertainty ellipse, are marked bold. If the changed isobar and the isobar in the partial wave are the same, the entry is underlined.

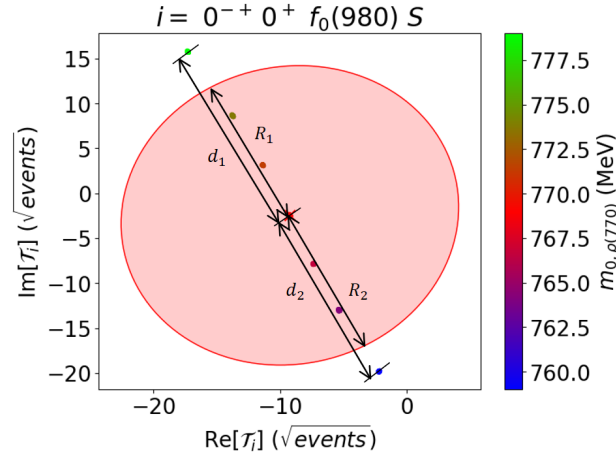


Figure 3.10: The figure shows the fit results with the definition of the length R_1 , R_2 , d_1 and d_2 .

Table 3.3: The maximal relative deviation Δ (see Eq. 3.1) for the fit results under isobar parameter changes of Monte Carlo data for $m_{3\pi} = 1.8 \text{ GeV}$

$J^{PC} M^{\xi} \text{ Isobar } L_{\xi\pi}$	$\rho(770)$		$f_2(1270)$		$f_0(1500)$		$\rho_3(1690)$	
	Δ_{m_0}	Δ_{Γ_0}	Δ_{m_0}	Δ_{Γ_0}	Δ_{m_0}	Δ_{Γ_0}	Δ_{m_0}	Δ_{Γ_0}
$0^{-+} 0^+ [\pi\pi]_S S$	0.341	0.128	0.062	0.176	4.687	0.290	0.046	0.028
$0^{-+} 0^+ \rho(770) P$	<u>0.877</u>	<u>0.108</u>	0.061	0.078	1.786	0.015	0.027	0.011
$0^{-+} 0^+ f_0(980) S$	0.493	0.121	0.049	0.171	4.923	0.059	0.040	0.023
$0^{-+} 0^+ f_2(1270) D$	0.463	0.170	<u>0.336</u>	<u>0.145</u>	0.571	0.040	0.029	0.017
$0^{-+} 0^+ f_0(1500) S$	0.331	0.031	0.097	0.086	<u>0.034</u>	<u>0.318</u>	0.035	0.006
$1^{++} 0^+ [\pi\pi]_S P$	0.427	0.269	0.254	0.106	1.129	0.046	0.045	0.020
$1^{++} 1^+ [\pi\pi]_S P$	0.275	0.195	0.216	0.015	0.325	0.022	0.024	0.009
$1^{++} 0^+ \rho(770) S$	<u>0.982</u>	<u>0.247</u>	0.103	0.143	1.946	0.032	0.016	0.015
$1^{++} 1^+ \rho(770) S$	<u>0.870</u>	<u>0.092</u>	0.135	0.118	1.508	0.043	0.020	0.008
$1^{++} 0^+ \rho(770) D$	<u>0.691</u>	<u>0.082</u>	0.154	0.129	1.638	0.017	0.010	0.003
$1^{++} 1^+ \rho(770) D$	1.036	<u>0.112</u>	0.117	0.138	1.841	0.044	0.008	0.007
$1^{++} 0^+ f_0(980) P$	0.203	0.055	0.083	0.010	0.575	0.015	0.018	0.002
$1^{++} 1^+ f_0(980) P$	0.056	0.075	0.119	0.049	0.284	0.018	0.012	0.003
$1^{++} 0^+ f_2(1270) P$	0.210	0.122	<u>0.424</u>	<u>0.055</u>	1.107	0.048	0.034	0.033
$1^{++} 1^+ f_2(1270) P$	0.136	0.081	<u>0.592</u>	<u>0.038</u>	1.684	0.048	0.019	0.012
$1^{++} 0^+ f_2(1270) F$	0.147	0.091	<u>0.107</u>	<u>0.174</u>	0.102	0.006	0.050	0.019
$1^{++} 0^+ \rho_3(1690) D$	0.296	0.204	0.028	0.114	0.802	0.021	<u>0.062</u>	<u>0.038</u>

Continued on next page

Table 3.3 – continued from previous page

$J^{PC} M^{\epsilon}$ Isobar $L_{\xi\pi}$	$\rho(770)$		$f_2(1270)$		$f_0(1500)$		$\rho_3(1690)$	
	Δ_{m_0}	Δ_{Γ_0}	Δ_{m_0}	Δ_{Γ_0}	Δ_{m_0}	Δ_{Γ_0}	Δ_{m_0}	Δ_{Γ_0}
$1^{++} 0^+ \rho_3(1690) G$	0.115	0.230	0.176	0.048	0.393	0.016	<u>0.024</u>	<u>0.015</u>
$1^{-+} 1^+ \rho(770) P$	<u>0.572</u>	<u>0.042</u>	0.103	0.090	0.920	0.003	0.017	0.012
$2^{++} 1^+ \rho(770) D$	<u>0.399</u>	<u>0.060</u>	0.130	0.052	0.154	0.025	0.019	0.006
$2^{++} 2^+ \rho(770) D$	<u>0.035</u>	<u>0.027</u>	0.144	0.073	0.372	0.014	0.004	0.009
$2^{++} 1^+ f_2(1270) P$	0.193	0.039	<u>0.327</u>	<u>0.067</u>	0.657	0.032	0.019	0.015
$2^{++} 2^+ f_2(1270) P$	0.063	0.063	<u>0.188</u>	<u>0.084</u>	0.181	0.007	0.002	0.007
$2^{++} 1^+ \rho_3(1690) D$	0.113	0.083	0.222	0.046	0.157	0.032	<u>0.035</u>	<u>0.041</u>
$2^{-+} 0^+ [\pi\pi]_S D$	0.092	0.123	0.676	0.507	1.427	0.062	0.024	0.009
$2^{-+} 1^+ [\pi\pi]_S D$	0.268	0.186	0.235	0.190	0.612	0.030	0.013	0.013
$2^{-+} 0^+ \rho(770) P$	<u>0.754</u>	<u>0.235</u>	0.517	0.154	2.108	0.048	0.018	0.006
$2^{-+} 1^+ \rho(770) P$	1.053	<u>0.156</u>	0.056	0.152	2.325	0.033	0.017	0.011
$2^{-+} 2^+ \rho(770) P$	<u>0.041</u>	<u>0.069</u>	0.038	0.037	0.177	0.017	0.009	0.001
$2^{-+} 0^+ \rho(770) F$	1.254	<u>0.099</u>	0.244	0.129	1.754	0.053	0.026	0.033
$2^{-+} 1^+ \rho(770) F$	<u>0.588</u>	<u>0.035</u>	0.082	0.025	1.147	0.026	0.017	0.027
$2^{-+} 0^+ f_0(980) D$	0.228	0.108	0.087	0.141	0.666	0.026	0.014	0.009
$2^{-+} 0^+ f_2(1270) S$	0.213	0.183	<u>0.815</u>	<u>0.311</u>	1.892	0.029	0.021	0.020
$2^{-+} 1^+ f_2(1270) S$	0.106	0.124	<u>0.564</u>	<u>0.076</u>	1.347	0.004	0.020	0.016
$2^{-+} 2^+ f_2(1270) S$	0.077	0.030	<u>0.333</u>	<u>0.030</u>	0.709	0.016	0.008	0.010
$2^{-+} 0^+ f_2(1270) D$	0.443	0.162	<u>0.692</u>	<u>0.159</u>	3.046	0.075	0.016	0.035
$2^{-+} 1^+ f_2(1270) D$	0.083	0.027	<u>0.279</u>	<u>0.042</u>	0.875	0.019	0.014	0.010
$2^{-+} 2^+ f_2(1270) D$	0.120	0.045	<u>0.131</u>	<u>0.074</u>	0.616	0.011	0.002	0.003
$2^{-+} 0^+ f_2(1270) G$	0.300	0.173	<u>0.374</u>	<u>0.120</u>	0.810	0.019	0.019	0.015
$2^{-+} 0^+ \rho_3(1690) P$	0.837	0.016	0.663	0.087	0.843	0.028	<u>0.072</u>	<u>0.104</u>
$2^{-+} 1^+ \rho_3(1690) P$	0.205	0.045	0.146	0.055	0.230	0.025	<u>0.068</u>	<u>0.046</u>
$3^{++} 0^+ [\pi\pi]_S F$	0.194	0.258	0.445	0.070	0.558	0.029	0.213	0.109
$3^{++} 1^+ [\pi\pi]_S F$	0.081	0.059	0.260	0.027	0.775	0.025	0.025	0.044
$3^{++} 0^+ \rho(770) D$	1.794	<u>0.158</u>	0.076	0.065	2.779	0.056	0.059	0.057
$3^{++} 1^+ \rho(770) D$	<u>0.851</u>	<u>0.145</u>	0.065	0.050	1.366	0.027	0.036	0.032
$3^{++} 0^+ \rho(770) G$	<u>0.765</u>	<u>0.097</u>	0.250	0.053	1.647	0.048	0.041	0.017
$3^{++} 1^+ \rho(770) G$	<u>0.500</u>	<u>0.041</u>	0.020	0.055	0.894	0.015	0.014	0.008
$3^{++} 0^+ f_2(1270) P$	0.084	0.278	<u>0.985</u>	<u>0.074</u>	2.287	0.055	0.097	0.076
$3^{++} 1^+ f_2(1270) P$	0.137	0.080	<u>0.556</u>	<u>0.100</u>	1.322	0.029	0.013	0.016
$3^{++} 0^+ \rho_3(1690) S$	0.391	0.214	0.273	0.121	1.425	0.066	<u>0.441</u>	<u>0.235</u>
$3^{++} 1^+ \rho_3(1690) S$	0.504	0.082	0.143	0.044	0.645	0.011	<u>0.158</u>	<u>0.151</u>
$3^{++} 0^+ \rho_3(1690) I$	0.447	0.092	0.095	0.068	0.173	0.017	<u>0.053</u>	<u>0.032</u>
$3^{-+} 1^+ \rho(770) F$	<u>0.293</u>	<u>0.020</u>	0.105	0.019	0.553	0.017	0.016	0.016

Continued on next page

Table 3.3 – continued from previous page

$J^{PC} M^{\epsilon}$ Isobar $L_{\xi\pi}$	$\rho(770)$		$f_2(1270)$		$f_0(1500)$		$\rho_3(1690)$	
	Δ_{m_0}	Δ_{Γ_0}	Δ_{m_0}	Δ_{Γ_0}	Δ_{m_0}	Δ_{Γ_0}	Δ_{m_0}	Δ_{Γ_0}
$3^{-+} 1^+ f_2(1270) D$	0.210	0.042	<u>0.457</u>	<u>0.064</u>	0.810	0.018	0.003	0.011
$4^{++} 1^+ \rho(770) G$	<u>0.953</u>	<u>0.038</u>	0.028	0.071	1.722	0.025	0.028	0.015
$4^{++} 2^+ \rho(770) G$	<u>0.093</u>	<u>0.046</u>	0.099	0.018	0.124	0.008	0.008	0.008
$4^{++} 1^+ f_2(1270) F$	0.106	0.044	<u>0.304</u>	<u>0.029</u>	1.190	0.015	0.028	0.013
$4^{++} 2^+ f_2(1270) F$	0.082	0.024	<u>0.056</u>	<u>0.030</u>	0.091	0.005	0.013	0.003
$4^{++} 1^+ \rho_3(1690) D$	0.191	0.179	0.089	0.075	0.396	0.011	<u>0.050</u>	<u>0.069</u>
$4^{-+} 0^+ [\pi\pi]_S G$	0.185	0.165	0.292	0.042	1.122	0.010	0.042	0.009
$4^{-+} 0^+ \rho(770) F$	1.310	<u>0.016</u>	0.303	0.103	2.001	0.049	0.040	0.010
$4^{-+} 1^+ \rho(770) F$	<u>0.438</u>	<u>0.104</u>	0.091	0.062	1.050	0.040	0.013	0.013
$4^{-+} 0^+ f_2(1270) D$	0.273	0.050	<u>0.350</u>	<u>0.116</u>	0.745	0.014	0.032	0.006
$4^{-+} 1^+ f_2(1270) D$	0.045	0.081	<u>0.310</u>	<u>0.040</u>	0.800	0.019	0.014	0.013
$4^{-+} 0^+ f_2(1270) G$	0.197	0.038	<u>0.123</u>	<u>0.106</u>	0.035	0.029	0.014	0.005
$5^{++} 0^+ [\pi\pi]_S H$	0.168	0.079	0.127	0.029	0.359	0.019	0.037	0.024
$5^{++} 1^+ [\pi\pi]_S H$	0.066	0.054	0.115	0.075	0.616	0.026	0.011	0.017
$5^{++} 0^+ \rho(770) G$	<u>0.287</u>	<u>0.108</u>	0.275	0.130	0.512	0.024	0.033	0.013
$5^{++} 0^+ f_2(1270) F$	0.062	0.087	<u>0.378</u>	<u>0.090</u>	0.764	0.015	0.039	0.023
$5^{++} 1^+ f_2(1270) F$	0.106	0.021	<u>0.429</u>	<u>0.009</u>	1.028	0.023	0.013	0.017
$5^{++} 0^+ f_2(1270) H$	0.167	0.039	<u>0.160</u>	<u>0.018</u>	0.496	0.011	0.013	0.005
$5^{++} 0^+ \rho_3(1690) D$	0.127	0.058	0.071	0.024	0.187	0.018	<u>0.022</u>	<u>0.030</u>
$6^{++} 1^+ \rho(770) I$	<u>0.173</u>	<u>0.016</u>	0.013	0.018	0.146	0.006	0.009	0.001
$6^{++} 1^+ f_2(1270) H$	0.151	0.068	<u>0.071</u>	<u>0.033</u>	0.123	0.005	0.015	0.007
$6^{-+} 0^+ [\pi\pi]_S I$	0.226	0.071	0.146	0.047	0.157	0.017	0.013	0.016
$6^{-+} 1^+ [\pi\pi]_S I$	0.128	0.077	0.153	0.064	0.887	0.016	0.002	0.005
$6^{-+} 0^+ \rho(770) H$	1.189	<u>0.027</u>	0.193	0.037	2.017	0.036	0.037	0.025
$6^{-+} 1^+ \rho(770) H$	<u>0.532</u>	<u>0.081</u>	0.059	0.037	0.992	0.005	0.012	0.004
$6^{-+} 0^+ f_2(1270) G$	0.235	0.077	<u>0.234</u>	<u>0.107</u>	0.300	0.005	0.016	0.016
$6^{-+} 0^+ \rho_3(1690) F$	0.335	0.082	0.133	0.013	0.661	0.043	<u>0.016</u>	<u>0.051</u>
$1^{++} 1^- \rho(770) S$	<u>0.022</u>	<u>0.064</u>	0.075	0.056	0.017	0.015	0.005	0.008
$1^{-+} 0^- \rho(770) P$	<u>0.267</u>	<u>0.133</u>	0.085	0.051	0.064	0.023	0.021	0.003
$1^{-+} 1^- \rho(770) P$	<u>0.215</u>	<u>0.134</u>	0.098	0.111	0.072	0.019	0.025	0.007
$2^{++} 0^- \rho(770) D$	<u>0.105</u>	<u>0.042</u>	0.081	0.038	0.042	0.019	0.003	0.006
$2^{++} 0^- f_2(1270) P$	0.220	0.068	<u>0.224</u>	<u>0.076</u>	0.035	0.050	0.010	0.021
$2^{++} 1^- f_2(1270) P$	0.202	0.061	<u>0.367</u>	<u>0.085</u>	0.056	0.009	0.011	0.004
$2^{-+} 1^- f_2(1270) S$	0.210	0.040	<u>0.150</u>	<u>0.076</u>	0.030	0.031	0.019	0.027
Flat	0.000	0.000	0.000	0.000	0.000	0.000	0.000	0.000
Maximum	1.794	0.278	0.985	0.507	4.923	0.318	0.441	0.235

Here, I divide the analysis to the following aspects:

1. Comparing the maxima of Δ , one finds changes of isobar masses affect more than their widths. For example, the change of $m_{0,\rho(770)}$ gives several partial waves with $\Delta > 1$, while the change of $\Gamma_{0,\rho(770)}$ gives only maximal 0.3. The previous analysis is positively supported. On the other hand, no clear pattern is found between the isobars. This may result from the scale of changes we chose: up to ± 10 MeV (an absolute scale) for all isobar parameters. We kept it fixed as a scale of the measurable mass resolution.
2. In ideal case, the partial waves are independent of each other. Isobars, partly defined the partial wave, should also give independent subspaces. Based on this hypothesis, larger Δ values are expected for the partial waves when their isobar is the same as the changed isobar. In table 3.3, these Δ are underlined. Compared these underlined entries to the non-underlined inside each block. I found:
 - i) For width shifts, the underlined values are not necessarily larger. So no clear pattern is found. This may be because of the small shift of width in general—There is even no single entry larger than one. In this case, statistical uncertainty plays an important role.
 - ii) For mass shifts, The underlined values are roughly dominant, however, with the exception $f_0(1500)$. The special role of $f_0(1500)$ will be discussed as follows.
3. Similarly, I expected for the quantum numbers a joint pattern. In table 3.3, the quantum numbers are classified by different blocks. However, the value inside each blocks fluctuate a lot, which is in disagreement of the expectation. Here, maybe the whole set of quantum numbers should be categorized, inclusive the orbital angular momentum $L_{\xi\pi}$. Yet, in this case, there are too many groups with too less entries for the 88 waves, which is not sufficient to find a common pattern. Therefore, a systematic analysis for the angular parts is impossible.
4. The $f_0(1500)$ mass changes yield irregular and often large shifts on transition amplitudes. The maximal value reaches $\Delta \approx 5$. The reason is that $f_0(1500)$ has the same $J^P = 0^+$ as $f_0(500)$ ($[\pi\pi]_S$) and $f_0(980)$. So correlation between these isobars is expected. In fact, the largest shifts of the fit results are indeed observed for the partial waves $0^{-+} 0^+ [\pi\pi]_S S$ ($\Delta = 4.687$) and $0^{-+} 0^+ f_0(980) S$ ($\Delta = 4.923$). However, for the partial wave $0^{-+} 0^+ f_0(1500) S$ only $\Delta = 0.034$ is found. This is the only partial wave with $f_0(1500)$, yet not susceptible to the changing parameter of $f_0(1500)$ at all. In addition, leakage effect is found at changes of $f_0(1500)$, while not observed by shift of the other

isobar parameters. For instance, on changing the mass of $f_0(1500)$, one finds the susceptibility ‘leaks’ to other isobars such as $\rho(770)$. (See, for example, the block of $J^{PC} = 1^{++}$.) It is important for us to be aware of this weirdness for the further analysis.

For $m_{3\pi} = 1.0 \text{ GeV}$, the analysis task is less sophisticated. As discussed before, the susceptibility of the transition amplitudes reduces drastically for all isobars with $m_{0,\xi} > m_{3\pi}$. According to table B.2, the small Δ for the isobar parameters’ changes except for $\rho(770)$ agree with the small susceptibility. In addition, the similar leakage effect is observed concerning $\rho(770)$ parameters’ changes. This is reasonable as it lost the independent components. The rest intensity has to be somehow distributed.

3.2.2 Shift of $-\log \mathcal{L}$ for the Best Fit Result

In this part, I evaluate the dependence of the $-\log \mathcal{L}$ value of the best result, defined as $-\log \mathcal{L}_{\text{best}}$, on the isobar parameters. As mentioned in section 3.1.3, for large number of events, $-\log \mathcal{L}$ is expected to be a parabola in the isobar parameters as model parameters. The reason why I performed the analysis for the Monte Carlo data first is to ensure the feasibility of this method.

To fit the $-\log \mathcal{L}_{\text{best}}$ dependence of the isobar parameters by 2nd-order polynomial is the clear goal. The trivial attempt would be fit it to a parabola considering all the isobar parameters. Empirically, to stabilize this fit, one need hundreds of ‘data points’. Here, each ‘data point’ means one fit result, where a elaborate fit algorithm stands behind. In this case, producing an amount of them would be very expensive. Besides, it is hard to judge the fit quality. One may get numeric outputs from the fit algorithm concerning the fit quality. Yet, since there is only one fit to be done, one lacks comparison for these numbers. Therefore, I should pursue a more simple way to attain our goal.

Empirically, the parameters of different isobars have small correlation among each other. Making use of this small correlation, I fitted the $-\log \mathcal{L}_{\text{best}}$ parabolic with changed parameters of each isobar, while keeping the other isobar parameters the reference values in table 3.1. This yields a 2nd-order polynomial surface in $m_{0,\xi}$ and $\Gamma_{0,\xi}$ for each isobar ξ . Compared to the single isobar parameters’ changes studied by the last section, I added 4 extra points on both mass and width shifts of each isobar to stabilize the parabola. The outcome of the fit is the apex of the parabola given by the minimum in case the coefficient of the quadratic term is positive. Before the results presented, the following two aspects still deserve our attention:

The Analysis Validity

Ideally, $-\log \mathcal{L}_{\text{best}}$ should be a 2D 2nd order polynomial in the $(m_{0,\xi}, \Gamma_{0,\xi})$ plane, however, only in case that the isobar does affect the fit. Similar to the transition amplitudes discussed in section 3.2.1 and table B.2, $-\log \mathcal{L}_{\text{best}}$ does not depend on parameters of isobars above the kinematic thresholds. For $m_{3\pi} = 1.0 \text{ GeV}$, these are all isobars except for the $\rho(770)$. The outcomes were in accordance with this expectation. For example, Fig. 3.11 shows plots of the parabolic fits for $\rho(770)$ parameters and $f_2(1270)$ parameters. To make the plots easier to read, the vertical axis was redefined as $\Delta \log \mathcal{L}_{\text{best}} = -\log \mathcal{L}_{\text{best}}(m_0, \Gamma_0) + \log \mathcal{L}_{\text{best}}(m_i, \Gamma_i)$.

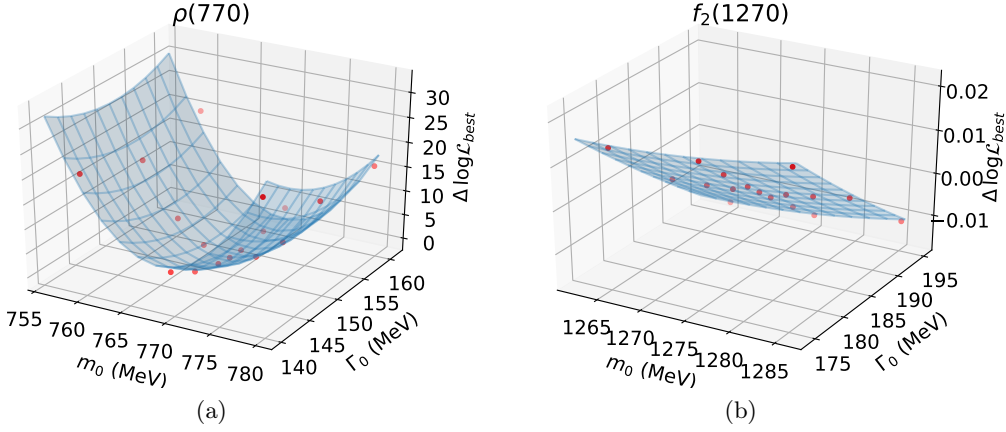


Figure 3.11: The figures show the $\Delta \log \mathcal{L}_{\text{best}}$ as a function of m_0 and Γ_0 (red points) and fitted 2nd-order polynomial (blue surface). They are generated from the Monte Carlo data with $m_{3\pi} = 1.0 \text{ GeV}$ concerning the change of $\rho(770)$ parameters (a) and $f_2(1270)$ parameters (b).

Here, for $\rho(770)$, one observes a typical parabolic shape, though the mass dependence is more drastic than the width. This is consistent with the outcomes in section 3.2.1: The transition amplitudes are affected more by shifts of isobar masses than their widths. For $f_2(1270)$, the surface is more like a plane. Focusing on the vertical axis, one sees the largest $\Delta \log \mathcal{L}_{\text{best}}$ only ranges up to 0.04, which is far too small compared to the analysis resolution represented by an elevation of 0.5 unit. In this case, it is not justified to read a result from that. So those isobars with their plot like this are excluded in the final results.

The Effect of Covariance between Mass and Width

I plotted the cross section of the 2D plots in each axis—mass and width. In this way, I got a 1D points set and a curve of the function value of our fitted parabola. Here, as reduced to 1-dimension, the data points can also be fitted to a 1-dimensional parabola. This new parabola may have different apex from the previous curve. Fig. 3.12 shows some examples.

The difference between the two fit curves is due to the covariance between the isobar mass and width. According to Fig. 3.12b and Fig. 3.12d, the difference between two fit curves indicates that the covariance does exist. Yet, although the covariance exists mutually between the isobar mass and width, the mass is much robuster on withstanding the effect of the correlation according to Fig. 3.12a and Fig. 3.12c. In analogous, the isobar masses may also withstand more covariance, for example, between parameters of different isobars. Therefore, the outcome mass parameters are more reliable.

Moreover, according to the plots of width dependence (Fig. 3.12b and Fig. 3.12d), the fit without considering the covariance evidently describes the data better, while the fits with this consideration give better results concerning the reference values (table 3.1). As these are the values using for generation of the data set, they are supposed to be the true values, so that the minimization of the parabola surface with consideration of the correlation between the isobar mass and width should give more reliable outcomes. In table 3.4, the results from both parabolic fits are presented. As for the uncertainties, I used the Gaussian assumption—the range with up to 0.5 unit elevation of $-\log \mathcal{L}_{\text{best}}$ is given.

For $m_{3\pi} = 1.8 \text{ GeV}$:				
Isobar	Parameter	reference value [MeV]	3D fit [MeV]	2D fit [MeV]
$\rho(770)$	m_0	769.0	769.4 ± 1.9	769.5 ± 1.9
	Γ_0	150.9	149.4 ± 4.0	148.5 ± 4.0
$f_2(1270)$	m_0	1275.1	1274.3 ± 2.6	1274.5 ± 2.6
	Γ_0	185.1	178.5 ± 5.5	177.9 ± 5.5
$f_0(1500)$	m_0	1505.0	1515.2 ± 9.1	1515.0 ± 9.1
	Γ_0	109.0	100.5 ± 15.0	101.0 ± 14.9
$\rho_3(1690)$	m_0	1688.8	1706.0 ± 18.6	1706.0 ± 18.6
	Γ_0	161.0	181.8 ± 29.0	185.0 ± 29.1
For $m_{3\pi} = 1.0 \text{ GeV}$:				
$\rho(770)$	m_0	769.0	769.2 ± 1.8	769.1 ± 1.8
	Γ_0	150.9	153.7 ± 3.6	152.6 ± 3.55

Table 3.4: Outcomes of parabolic fits of Monte Carlo data

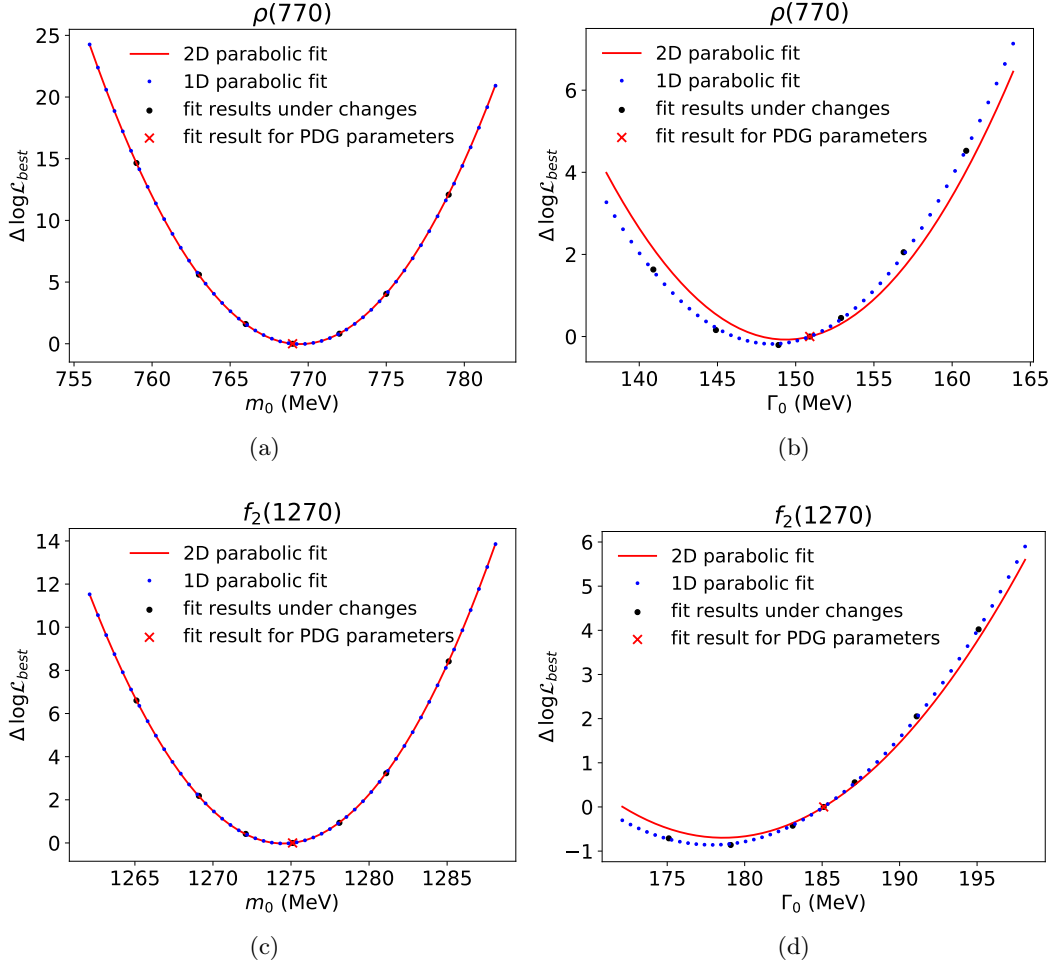


Figure 3.12: The figures shows the $\Delta \log \mathcal{L}_{\text{best}}$ on isobar changes as data points and two different parabolic fits. They are generated from the Monte Carlo data with $m_{3\pi} = 1.8 \text{ GeV}$ concerning the change of $m_{0,\rho(770)}$ (a), $\Gamma_{0,\rho(770)}$ (b), $m_{0,f_2(1270)}$ (c) and $\Gamma_{0,f_2(1270)}$ (d). 2D parabolic fits represent the cross section of the 2D parabola surface. 1D parabolic fits show the parabola directly fitted to the data points.

As summarized in table 3.4, these results and the reference parameters from table 3.1 are generally in good agreement. The larger uncertainties in widths than in masses agree with Fig. 3.11a. Besides, as the isobar mass increases, the deviation and the uncertainty both become larger. It is fair to say a larger uncertainty brings a larger deviation, and the uncertainty suggests the susceptibility—a larger uncertainty area indicates a flatter parabola. A flat likelihood w.r.t. one parameter, as a reference to the probability density, refers to how this parameter affects the fit. Here, at last, it is fair to compare between the isobars: According to the uncertainties of the outcomes, $\rho(770)$ and $f_2(1270)$ should be the dominant isobars.

This statement is true, according to previous analysis results of the COMPASS experiment. Looking to the $m_{2\pi}$ mass spectrum of the real experimental data (Fig. 3.13), we see clearer peaks for this two isobars in comparison to the other. In addition, the relative intensity variation between different partial waves can also be a good hint (Table 5 in Ref. [2]). There is a single partial wave, $1^{++} 0^+ \rho(770) S$, holding over 30% of the whole intensity while all other waves less than 10%. This gives the dominant weight of $\rho(770)$.

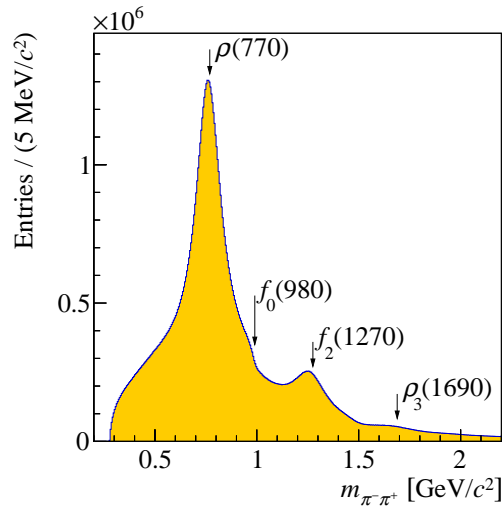


Figure 3.13: The figure shows the $m_{\pi\pi}$ mass spectrum [2].

Till here, I confirmed that the method of parabolic fitting $-\log \mathcal{L}_{\text{best}}$ concerning the isobar parameter changes works. In the next chapter, I will apply this method to the real data.

Chapter 4

Analysis for the Real Data

In this chapter, I analyze two real experimental data sets with $m_{3\pi}$ between 1.80 and 1.82 GeV, and between 1.00 and 1.02 GeV. Both data sets are with t' between 0.1 and 0.113 GeV². As discussed in section 2.2.1, for narrow bins of these two parameters, I regard them as constants with $m_{3\pi} = 1.8$ GeV and $m_{3\pi} = 1.0$ GeV and apply our model in Eq. (2.2) that describes the intensity as a function of the phase space variables τ .

For the real data, I focus primarily on estimating the optimal isobar parameters via the change of $-\log \mathcal{L}_{\text{best}}$. The chapter is divided into two parts. The first part will focus on the prerequisites of the analysis. In the second part, I will present and discuss the estimated isobar parameters.

4.1 Preparation

As the methodology is analog to the previous analysis of the Monte Carlo data (see chapter 3), only noticeable differences are shown as follows:

Modalities of the fit

The fit results of the data set with $m_{3\pi} = 1.8$ GeV is similar to the Monte Carlo data with $m_{3\pi} = 1.8$ GeV. For the data with $m_{3\pi} = 1.0$ GeV, difference appears. As discussed before, thresholds are necessary to stabilize the fit. However, thresholds do not exist in nature, and we want to use the same wave list for the both data sets to make better comparison. Hence, I analyzed the data with the PWA model without thresholds.

Thresholds benefit the fit stability. For comparing the $-\log \mathcal{L}_{\text{best}}$ value, the fit stability and the modality of each $-\log \mathcal{L}$ are not so important. So using the model with thresholds is primarily justified. Yet, for the algorithm, what does matter is that the $-\log \mathcal{L}$ does has a well-defined global minimum and I should be able to find it. This can be studied by performing the fit multiple time using random initial

values. For example, Fig 4.1a shows the histogram of $\Delta \log \mathcal{L} = -\log \mathcal{L} + \log \mathcal{L}_{\text{best}}$ in the range of statistical uncertainty, $\Delta \log \mathcal{L} < 0.5$, from totally about a thousand fit results.

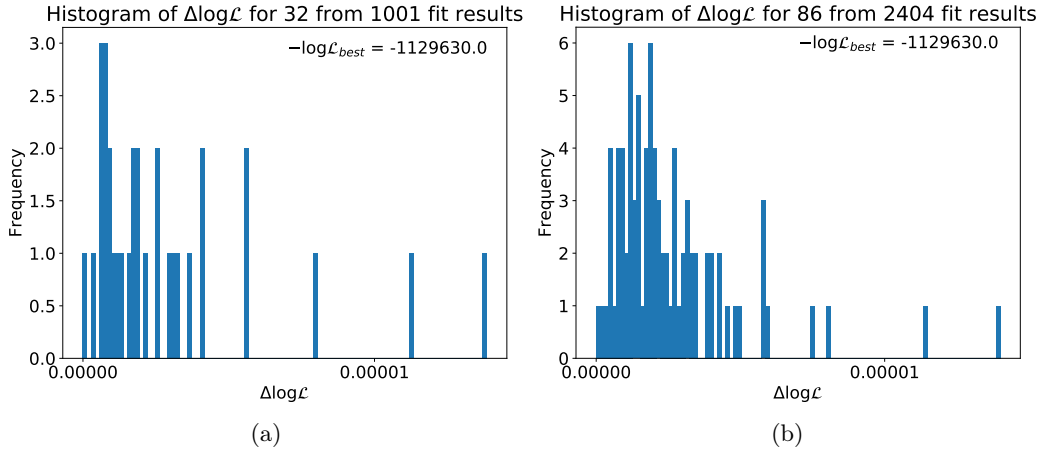


Figure 4.1: The figures show the $\Delta \log \mathcal{L}$ distribution for the real experimental data with $m_{3\pi}$ between 1.00 and 1.02 GeV. The fit model took the isobar parameters in table 3.1 and the partial-wave list without thresholds.

Here, the $\Delta \log \mathcal{L}$ ranges only over about 10^{-5} . The minimum is thus well-defined. However, there are only 32 fit results from a thousand that fall into the $\Delta \log \mathcal{L} < 0.5$ region. This proportion is too low for us to figure out whether it only represents a local minimum or the global one. Yet, as the initial value of the minimization distributed randomly, one can regard it as a random variable with a probability distribution. So in limit of infinity fit attempts, the probability that the logarithm can find the global minimum should go into constant. In this case, if the fit does find the global minimum, this proportion should represent this probability and go stable as the total amount of fit attempt increases. To prove that, I performed the algorithm for more times and plotted the outcome histogram in Fig 4.1b.

According to the two figures in Fig. 4.1, the two outcomes are in consistence. On one hand, the proportions are already in consistent: $32/1001 \approx 86/2404 \approx 0.3$. On the other hand, the lowest $-\log \mathcal{L}$ values that they captured are the same. Consequently, the minimization of about a thousand times does find the best fit result and will be applied for the further analysis.

Fit with changed isobar parameters: Shift of transition amplitudes

Strictly speaking, this part is not related to the final goal, as the $-\log \mathcal{L}_{\text{best}}$ distribution is independent of the distribution of each $-\log \mathcal{L}$ function itself. So, only superficial disparities between the results of the real data and the Monte Carlo data are shown.

In general, nothing noticeable is found concerning $m_{3\pi} = 1.8 \text{ GeV}$ (for example, Fig. 4.2a). For $m_{3\pi} = 1.0 \text{ GeV}$, there are some differences. Fig. 4.2b shows an example of the fit results. Firstly, the linearity of the shifts of the transition amplitudes does not survive. Besides, for the lowest $m_{0,\rho(770)}$, two solutions are found by the fit. As only the results within 0.5 unit elevation of $-\log \mathcal{L}$ were taken into account to the plots, we obtained here two good fit results indistinguishable in terms of the statistical uncertainty.

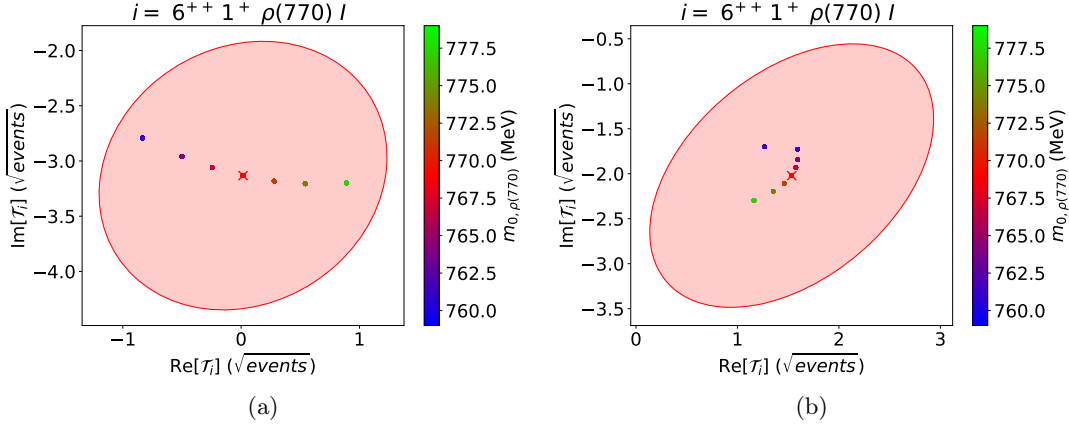


Figure 4.2: The figure shows the transition amplitude of a partial wave for PWA fits to real data with different values of the isobar parameters. Panel (a) is with higher $m_{3\pi}$: between 1.80 and 1.82 GeV and panel (b) with lower $m_{3\pi}$: between 1.00 and 1.02 GeV.

4.2 Results and Discussion

Up to now, I assured the feasibility of the analysis method. After performing the same scan process as in section 3.2.2, I got the results for the real data as presented in table 4.1. Here, the deviations to the PDG parameters larger than for the Monte

Carlo data. In particular, I marked the values with large deviations. For some of them, I extended the ranges of the input parameters to make sure the minimums are indeed in this position. I will discuss the outcomes as follows

For $m_{3\pi} = 1.8$ GeV:				
Isobar	Parameter	PDG value [MeV]	2D fit [MeV]	1D fit [MeV]
$\rho(770)$	m_0	769.0 ± 0.9	764.4 ± 1.0	765.6 ± 1.0
	Γ_0	150.9 ± 1.7	134.0 ± 2.3	134.5 ± 2.3
$f_2(1270)$	m_0	1275.1 ± 1.2	1277.6 ± 1.5	1277.6 ± 1.5
	Γ_0	$185.1^{+2.9}_{-2.4}$	189.0 ± 2.9	188.4 ± 2.9
$f_0(1500)$	m_0	1505.0 ± 6.0	-	-
	Γ_0	109.0 ± 7.0	-	-
$\rho_3(1690)$	m_0	1688.8 ± 2.1	1658.7 ± 8.3	1657.2 ± 8.4
	Γ_0	161.0 ± 10.0	133.9 ± 16.9	123.9 ± 18.7
For $m_{3\pi} = 1.0$ GeV:				
$\rho(770)$	m_0	769.0 ± 0.9	760.8 ± 1.1	761.7 ± 1.1
	Γ_0	150.9 ± 1.7	144.0 ± 1.8	147.0 ± 1.8

Table 4.1: Outcomes of parabolic fits of the real data

For $m_{3\pi} = 1.0$ GeV

Despite of the instability of the fit result due to removed thresholds, the outcomes for $\rho(770)$ parameters are pretty reliable. The other three isobars are subthresholded, so that their parameters cannot be extracted. Even though, the successful measurement of $\rho(770)$ parameters consoles us, that the fit algorithm without thresholds does work. The resultant plots can be found in Fig. 4.4 (a) and (b).

For $m_{3\pi} = 1.8$ GeV: $\rho(770)$ and $f_2(1270)$

Here, the parabolic fits work well (Fig. 4.4). The parabolic shape of $-\log \mathcal{L}_{\text{best}}$ distribution lends credence to the outcomes, however, with a relative large deviation on $\Gamma_{0,\rho(770)}$ (marked in table 4.1). This deviation may come from our model assumption that the isobar and the bachelor pion do not interact with each other (Fig. 2.2). A possible final state interaction between the $\rho(770)$ and bachelor pion may cause this deviation.

Another possible reason could be correlations with the parameters of other isobars. As the $\rho(770)$ and $f_2(1270)$ parameters were well-defined in this analysis and these are two isobars that affect most (Fig. 3.13), I checked the influence of their correlation

by fitting the $-\log \mathcal{L}_{\text{best}}$ dependent of $m_{0,\rho(770)}$, $\Gamma_{0,\rho(770)}$, $m_{0,f_2(1270)}$ and $\Gamma_{0,f_2(1270)}$ to a 4-dimensional parabola. The outcomes for the real data with $m_{3\pi} = 1.8 \text{ GeV}$ are:

$m_{0,\rho(770)}$ [MeV]	$\Gamma_{0,\rho(770)}$ [MeV]	$m_{0,f_2(1270)}$ [MeV]	$\Gamma_{0,f_2(1270)}$ [MeV]
764.3 ± 1.0	134.3 ± 2.3	1277.8 ± 1.5	189.23 ± 2.9

The results are similar to the measured parameters in table 4.1. Hence the correlation among these four parameters is not the reason for the deviation.

For $m_{3\pi} = 1.8 \text{ GeV}$: $f_0(1500)$

Fig. 4.3a and 4.3b show the $-\log \mathcal{L}_{\text{best}}$ as a function of the parameters of $f_0(1500)$. I think it is meaningless to extract $f_0(1500)$ parameters from these plots. On one hand, 1D fits yielded parameters far away from PDG, so that we can hardly lend credence to them. On the other hand, 2D fit did not work. As discussed in section 3.2.1, $f_0(1500)$ already showed a exotic property due to its ‘cross talk’ to parameters of other isobars. This may prevent reliable extraction of $f_0(1500)$ parameters.

For $m_{3\pi} = 1.8 \text{ GeV}$: $\rho_3(1690)$

For the $\rho_3(1690)$ parameters, I obtained relative good fitted parabolas (Fig. 4.3c and 4.3d), so that the outcomes should be meaningful, although with large deviations similar to the large uncertainty range. The reason for them could be the correlations among the isobars, as the deviations between the input isobar parameters from PDG and our parameters, in particular for $\Gamma_{0,\rho(770)}$, may cause the application of improper subspace of isobar parameters in the fits. If this reason be true, the deviations should be alleviated on performing a higher-dimensional fit. However, as I brought the $\rho(770)$ and $f_2(1270)$ parameters together as a test, no clear differences were found. Besides, the deviation can also exactly result from the large uncertainty. In the 2π mass spectrum (Fig. 3.13), almost no visible peak can be found for $\rho_3(1690)$, so that the amount of captured events may not be sufficient to fix its parameters.

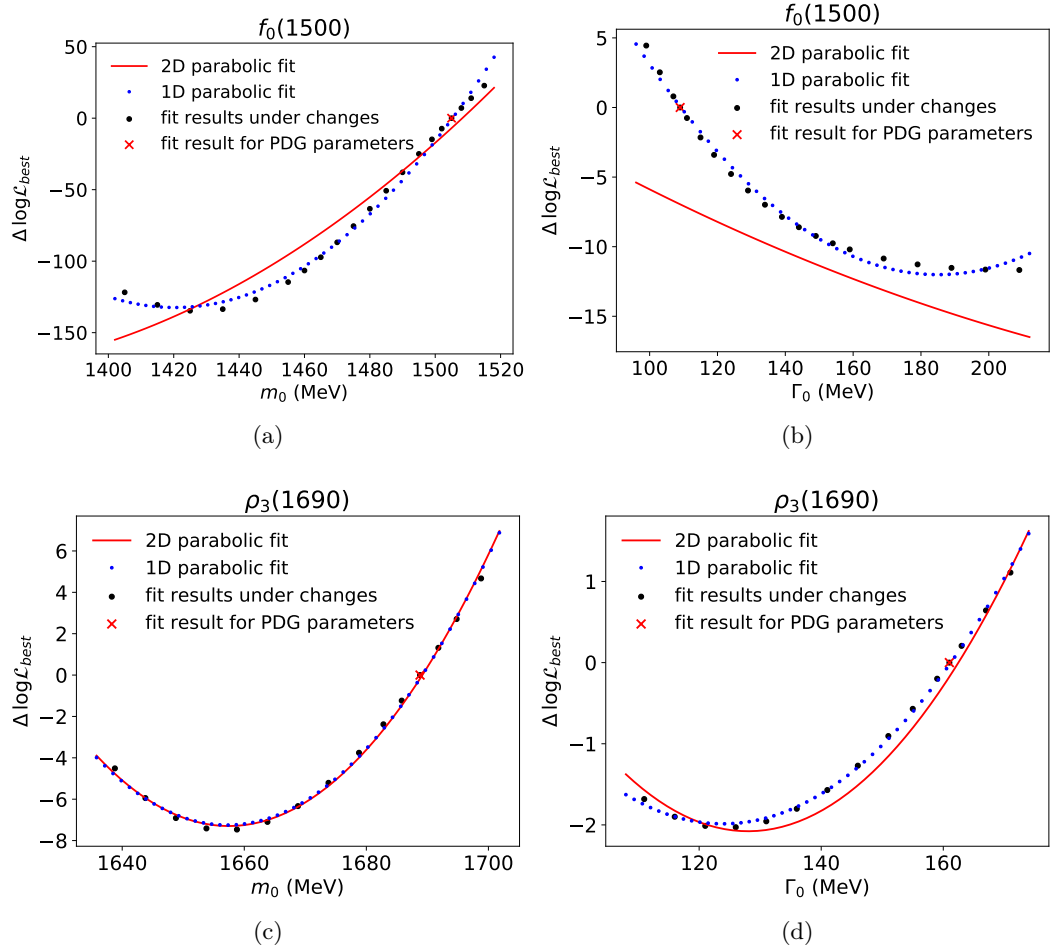
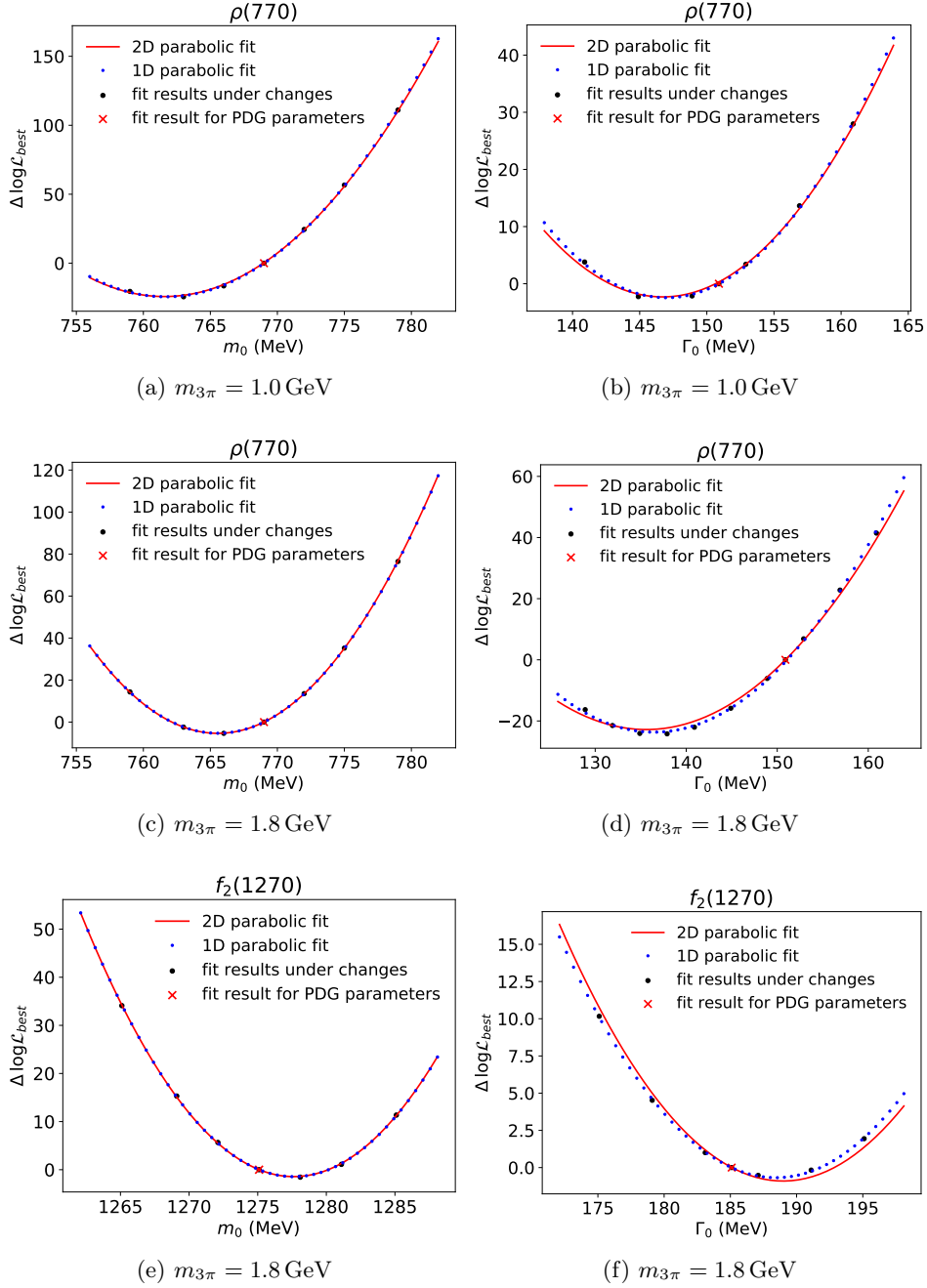


Figure 4.3: The figures show the $\Delta \log \mathcal{L}_{\text{best}}$ scans dependent of isobar parameters for real experimental data with $m_{3\pi}$ between 1.80 and 1.82 GeV.


 Figure 4.4: The figures show the $\Delta \log \mathcal{L}_{\text{best}}$ scans dependent of isobar parameters.

Chapter 5

Conclusions

In this thesis, I studied the partial-wave analysis results under changes of the isobar parameters for the reaction $\pi^- + p \rightarrow \pi^- + \pi^- + \pi^+ + p_{\text{recoil}}$. The analysis model was based on a previous analysis [2] and was fitted to the data using maximum likelihood method. Isobars, defined by mass and width parameters, describe the 2π subsystem in the successive 3π decay. I extracted the isobar parameters for two example $m_{3\pi}$ bins using $-\log \mathcal{L}$ scan. These isobar parameters are helpful for the ongoing analysis of data from the COMPASS experiment, as in this way we give our own measurements of the isobar parameters considering the individual interactions in our experiment.

Firstly, I analyzed Monte Carlo data generated by the best fit result of the real experimental data to evaluate the fit model. I discussed the fit performance under isobar parameter changes up to 10 MeV. The fit remained stable. Our model is robust under isobar parameter changes. In detail, I regarded the following two aspects: On one hand, the transition amplitudes shifted approximately linear with the isobar parameter changes. I evaluated and compared the shift in different aspects of data: For different $m_{3\pi}$, the fits are only susceptible to the isobar ξ with $m_\xi < m_{3\pi}$. The fit results shift in general more on masses changes than widths. For different partial waves, the isobar changes affect more those waves with the same isobar. The only exception is the $f_0(1500)$. No evident pattern was found in terms of the quantum numbers of the waves. On the other hand, I scanned the $-\log \mathcal{L}$ of the best fit results under isobar parameter changes to make sure this method works. Here, I confirmed that $-\log \mathcal{L}_{\text{best}}$ is in good approximation a parabola in the isobar parameters. The apex of the parabola were successfully located near the inputted parameters so that the method does work.

Subsequently, I scanned the $-\log \mathcal{L}$ of the best fit results of the real experimental data. To make sure I can find the best fit results, i.e. the global minimum of $-\log \mathcal{L}$, I analyzed the $-\log \mathcal{L}$ histogram and argued the feasibility. The shifts of transition amplitude were shortly discussed as I found multimodality of the $-\log \mathcal{L}$ of real data with $m_{3\pi} = 1.0 \text{ GeV}$ with a lighter $\rho(770)$ mass. Then, I performed the scan and

extracted the parameters of $\rho(770)$, $f_2(1270)$ and $\rho_3(1690)$ (table 4.1). In general, the $f_2(1270)$ parameters agree with the PDG averages. The parameters for $\rho(770)$ and $\rho_3(1690)$ deviate from the PDG averages, which could be a sign for effects from final-state interactions of ρ and ρ_3 with the bachelor pion.

Chapter 6

Outlook

Here, I follow some aspects that what can still be done in terms of the frame of the previous analysis:

Firstly, concerning the most useful part of the analysis, I extracted the isobar parameters from the experimental data that are in some case different from the PDG parameters. This is a bit strange, but still in our expectation, as the PDG parameters came from the averaging results of various of experiments. In our experiment, the results may be affected by the interaction of the outgoing particles or non-resonance contributions, which other experiments did not have. In this case, we may lend more credence to our own isobar parameters. Meanwhile, as we studied, the deviation of the input isobar parameters does influence the fit results in terms of the real experimental data (Fig. 4.2b). Thus, it would be interesting, for example, to substitute our input isobar parameters to our predicted values and to see whether the outcome $-\log \mathcal{L}$ function would be better (e.g. more stable, less modal values). However, this tool has its constraint for the two example experimental data set I used. That is, we are not able to find all the isobar parameters for a lower $m_{3\pi}$ due to their indistinguishable performance by the fit, and for a higher $m_{3\pi}$ the $-\log \mathcal{L}$ already has a single minimum due to the robustness of the model (shown in Chapter 3), so that the fit quality can be hard to compare between different isobar parameter sets. Still, the method may work for the data set with $m_{3\pi}$ between them. Besides, there are other ways to get our own isobar parameters (For example, Ref. [12]), so that this idea can be tested.

Secondly, I took the data of two different $m_{3\pi}$ as examples. I found, for instance for $\Gamma_{0,\rho(770)}$, that the measured isobar parameters can be different. This is interesting because it may reveal that final-state interactions affect the reaction differently in different 3π invariant mass. What can still be done is to extract the measured isobar parameters as a function of $m_{3\pi}$. The tendency can be interesting and this process is not so expensive as the algorithm is the same.

Finally, concerning the analysis detail, there are still parameters of two isobars that

remained unchanged and were not studied. On one hand, due to their exotic properties, the Breit-Wigner parameterization introduced large deviations of their $m_{\pi\pi}$ spectrum of the propagator term. On the other hand, other decay modes of the f_0 isobar may lead to other peaks of its spectrum, so that other parameters may still have to be added concerning these isobars. The study may go more complicated, but still feasible. Hence, if we would like to study the model more comprehensively, we can still take them into account.

Appendix A

Isobar Parameterizations

$\rho(770)$:

mass: Eq.(2.6)

width:

$$\Gamma(m) = \Gamma_0 \frac{q}{q_0} \frac{F_{Lr}^2(q)}{F_{Lr}^2(q_0)} \quad (\text{A.1})$$

where q and q_0 are defined as in Eq.(2.7).

$f_2(1270)$:

mass: Eq.(2.6)

width: Eq.(2.7)

$f_0(1500)$:

mass: Eq.(2.6)

width:

$$\Gamma = \Gamma_0 \quad (\text{A.2})$$

$\rho_3(1690)$:

mass:

$$\Delta(m; m_0, \Gamma_0) = \frac{\sqrt{mm_0} \Gamma_0}{m_0^2 - m^2 - im_0 \Gamma(m)} \quad (\text{A.3})$$

width:

$$\Gamma = \Gamma_0 \quad (\text{A.4})$$

Appendix B

Large Tables

Table B.1: Wave list for the fits. 80 waves with positive reflectivity, 7 with negative, plus an incoherent isotropic wave [2].

$J^{PC} M^e$	Isobar	$L_{\xi\pi}$	Threshold [MeV]
$0^{-+} 0^+$	$[\pi\pi]_S$	S	—
$0^{-+} 0^+$	$\rho(770)$	P	—
$0^{-+} 0^+$	$f_0(980)$	S	1200
$0^{-+} 0^+$	$f_2(1270)$	D	—
$0^{-+} 0^+$	$f_0(1500)$	S	1700
$1^{++} 0^+$	$[\pi\pi]_S$	P	—
$1^{++} 1^+$	$[\pi\pi]_S$	P	1100
$1^{++} 0^+$	$\rho(770)$	S	—
$1^{++} 1^+$	$\rho(770)$	S	—
$1^{++} 0^+$	$\rho(770)$	D	—
$1^{++} 1^+$	$\rho(770)$	D	—
$1^{++} 0^+$	$f_0(980)$	P	1180
$1^{++} 1^+$	$f_0(980)$	P	1140
$1^{++} 0^+$	$f_2(1270)$	P	1220
$1^{++} 1^+$	$f_2(1270)$	P	—
$1^{++} 0^+$	$f_2(1270)$	F	—
$1^{++} 0^+$	$\rho_3(1690)$	D	—
$1^{++} 0^+$	$\rho_3(1690)$	G	—
$1^{-+} 1^+$	$\rho(770)$	P	—
$2^{++} 1^+$	$\rho(770)$	D	—
$2^{++} 2^+$	$\rho(770)$	D	—
$2^{++} 1^+$	$f_2(1270)$	P	1000
$2^{++} 2^+$	$f_2(1270)$	P	1400
$2^{++} 1^+$	$\rho_3(1690)$	D	800
$2^{-+} 0^+$	$[\pi\pi]_S$	D	—

Continued on next page

Table B.1 – continued from previous page

$J^{PC} M^\varepsilon$	Isobar	$L_{\xi\pi}$	Threshold [MeV]
$2^{-+} 1^+$	$[\pi\pi]_S$	D	—
$2^{-+} 0^+$	$\rho(770)$	P	—
$2^{-+} 1^+$	$\rho(770)$	P	—
$2^{-+} 2^+$	$\rho(770)$	P	—
$2^{-+} 0^+$	$\rho(770)$	F	—
$2^{-+} 1^+$	$\rho(770)$	F	—
$2^{-+} 0^+$	$f_0(980)$	D	1160
$2^{-+} 0^+$	$f_2(1270)$	S	—
$2^{-+} 1^+$	$f_2(1270)$	S	1100
$2^{-+} 2^+$	$f_2(1270)$	S	—
$2^{-+} 0^+$	$f_2(1270)$	D	—
$2^{-+} 1^+$	$f_2(1270)$	D	—
$2^{-+} 2^+$	$f_2(1270)$	D	—
$2^{-+} 0^+$	$f_2(1270)$	G	—
$2^{-+} 0^+$	$\rho_3(1690)$	P	1000
$2^{-+} 1^+$	$\rho_3(1690)$	P	1300
$3^{++} 0^+$	$[\pi\pi]_S$	F	1380
$3^{++} 1^+$	$[\pi\pi]_S$	F	1380
$3^{++} 0^+$	$\rho(770)$	D	—
$3^{++} 1^+$	$\rho(770)$	D	—
$3^{++} 0^+$	$\rho(770)$	G	—
$3^{++} 1^+$	$\rho(770)$	G	—
$3^{++} 0^+$	$f_2(1270)$	P	960
$3^{++} 1^+$	$f_2(1270)$	P	1140
$3^{++} 0^+$	$\rho_3(1690)$	S	1380
$3^{++} 1^+$	$\rho_3(1690)$	S	1380
$3^{++} 0^+$	$\rho_3(1690)$	I	—
$3^{-+} 1^+$	$\rho(770)$	F	—
$3^{-+} 1^+$	$f_2(1270)$	D	1340
$4^{++} 1^+$	$\rho(770)$	G	—
$4^{++} 2^+$	$\rho(770)$	G	—
$4^{++} 1^+$	$f_2(1270)$	F	—
$4^{++} 2^+$	$f_2(1270)$	F	—
$4^{++} 1^+$	$\rho_3(1690)$	D	1700
$4^{-+} 0^+$	$[\pi\pi]_S$	G	1400
$4^{-+} 0^+$	$\rho(770)$	F	—
$4^{-+} 1^+$	$\rho(770)$	F	—
Continued on next page			

Table B.1 – continued from previous page

$J^{PC} M^\epsilon$	Isobar	$L_{\xi\pi}$	Threshold [MeV]
$4^{-+} 0^+$	$f_2(1270)$	D	—
$4^{-+} 1^+$	$f_2(1270)$	D	—
$4^{-+} 0^+$	$f_2(1270)$	G	1600
$5^{++} 0^+$	$[\pi\pi]_S$	H	—
$5^{++} 1^+$	$[\pi\pi]_S$	H	—
$5^{++} 0^+$	$\rho(770)$	G	—
$5^{++} 0^+$	$f_2(1270)$	F	980
$5^{++} 1^+$	$f_2(1270)$	F	—
$5^{++} 0^+$	$f_2(1270)$	H	—
$5^{++} 0^+$	$\rho_3(1690)$	D	1360
$6^{++} 1^+$	$\rho(770)$	I	—
$6^{++} 1^+$	$f_2(1270)$	H	—
$6^{-+} 0^+$	$[\pi\pi]_S$	I	—
$6^{-+} 1^+$	$[\pi\pi]_S$	I	—
$6^{-+} 0^+$	$\rho(770)$	H	—
$6^{-+} 1^+$	$\rho(770)$	H	—
$6^{-+} 0^+$	$f_2(1270)$	G	—
$6^{-+} 0^+$	$\rho_3(1690)$	F	—
$1^{++} 1^-$	$\rho(770)$	S	—
$1^{-+} 0^-$	$\rho(770)$	P	—
$1^{-+} 1^-$	$\rho(770)$	P	—
$2^{++} 0^-$	$\rho(770)$	D	—
$2^{++} 0^-$	$f_2(1270)$	P	1180
$2^{++} 1^-$	$f_2(1270)$	P	1300
$2^{-+} 1^-$	$f_2(1270)$	S	—
Flat			—

Table B.2: The maximal relative deviation for the best fit results under each single isobar parameter change of Monte Carlo data for $m_{3\pi} = 1.0$ GeV

$J^{PC} M^{\xi} \text{ Isobar } L_{\xi\pi}$	$\rho(770)$		$f_2(1270)$		$f_0(1500)$		$\rho_3(1690)$	
	Δ_{m_0}	Δ_{Γ_0}	Δ_{m_0}	Δ_{Γ_0}	Δ_{m_0}	Δ_{Γ_0}	Δ_{m_0}	Δ_{Γ_0}
$0^{-+} 0^+ [\pi\pi]_S S$	1.106	0.316	0.002	0.007	0.004	0.003	0.001	0.001
$0^{-+} 0^+ \rho(770) P$	1.468	<u>0.141</u>	0.015	0.008	0.002	0.000	0.001	0.001
$0^{-+} 0^+ f_0(980) S$	1.237	0.868	0.008	0.007	0.004	0.003	0.000	0.000
$0^{-+} 0^+ f_2(1270) D$	0.701	0.840	<u>0.004</u>	<u>0.010</u>	0.002	0.000	0.001	0.001
$0^{-+} 0^+ f_0(1500) S$	0.457	0.681	0.005	0.007	<u>0.006</u>	<u>0.002</u>	0.001	0.001
$1^{++} 0^+ [\pi\pi]_S P$	5.432	0.897	0.009	0.007	0.001	0.000	0.003	0.001
$1^{++} 1^+ [\pi\pi]_S P$	1.466	0.464	0.014	0.006	0.001	0.000	0.001	0.001
$1^{++} 0^+ \rho(770) S$	<u>0.390</u>	<u>0.476</u>	0.012	0.002	0.001	0.000	0.001	0.001
$1^{++} 1^+ \rho(770) S$	<u>0.577</u>	<u>0.402</u>	0.013	0.011	0.001	0.000	0.001	0.000
$1^{++} 0^+ \rho(770) D$	2.360	<u>0.418</u>	0.020	0.009	0.001	0.000	0.002	0.001
$1^{++} 1^+ \rho(770) D$	<u>0.598</u>	<u>0.324</u>	0.006	0.006	0.000	0.000	0.001	0.000
$1^{++} 0^+ f_0(980) P$	2.970	0.186	0.015	0.008	0.001	0.000	0.005	0.001
$1^{++} 1^+ f_0(980) P$	1.762	0.267	0.021	0.005	0.001	0.000	0.000	0.001
$1^{++} 0^+ f_2(1270) P$	1.918	0.916	<u>0.018</u>	<u>0.009</u>	0.001	0.000	0.002	0.001
$1^{++} 1^+ f_2(1270) P$	0.423	0.385	<u>0.013</u>	<u>0.024</u>	0.000	0.000	0.001	0.001
$1^{++} 0^+ f_2(1270) F$	2.798	1.004	<u>0.024</u>	<u>0.005</u>	0.001	0.000	0.002	0.000
$1^{++} 0^+ \rho_3(1690) D$	2.818	0.354	0.012	0.012	0.000	0.000	<u>0.003</u>	<u>0.001</u>
$1^{++} 0^+ \rho_3(1690) G$	0.922	0.581	0.015	0.009	0.001	0.001	<u>0.003</u>	<u>0.001</u>
$1^{-+} 1^+ \rho(770) P$	1.165	<u>0.421</u>	0.011	0.004	0.000	0.000	0.002	0.000
$2^{++} 1^+ \rho(770) D$	<u>0.409</u>	<u>0.106</u>	0.024	0.021	0.000	0.000	0.001	0.001
$2^{++} 2^+ \rho(770) D$	<u>0.254</u>	<u>0.106</u>	0.010	0.003	0.000	0.000	0.001	0.000
$2^{++} 1^+ f_2(1270) P$	1.091	0.217	<u>0.025</u>	<u>0.040</u>	0.000	0.000	0.001	0.000
$2^{++} 2^+ f_2(1270) P$	0.294	0.151	<u>0.009</u>	<u>0.002</u>	0.000	0.000	0.001	0.000
$2^{++} 1^+ \rho_3(1690) D$	0.966	0.090	0.005	0.003	0.000	0.000	<u>0.002</u>	<u>0.001</u>
$2^{-+} 0^+ [\pi\pi]_S D$	0.831	0.335	0.011	0.003	0.001	0.000	0.003	0.001
$2^{-+} 1^+ [\pi\pi]_S D$	0.689	0.538	0.000	0.007	0.000	0.000	0.002	0.001
$2^{-+} 0^+ \rho(770) P$	<u>0.525</u>	<u>0.149</u>	0.014	0.004	0.001	0.000	0.000	0.001
$2^{-+} 1^+ \rho(770) P$	<u>0.983</u>	<u>0.298</u>	0.004	0.007	0.000	0.000	0.002	0.001
$2^{-+} 2^+ \rho(770) P$	<u>0.274</u>	<u>0.039</u>	0.004	0.004	0.000	0.000	0.000	0.000
$2^{-+} 0^+ \rho(770) F$	<u>0.532</u>	<u>0.069</u>	0.013	0.006	0.001	0.000	0.000	0.000
$2^{-+} 1^+ \rho(770) F$	<u>0.975</u>	<u>0.184</u>	0.008	0.010	0.000	0.000	0.002	0.001
$2^{-+} 0^+ f_0(980) D$	0.688	0.279	0.015	0.004	0.001	0.000	0.003	0.001
$2^{-+} 0^+ f_2(1270) S$	0.750	0.298	<u>0.018</u>	<u>0.015</u>	0.001	0.000	0.001	0.001
$2^{-+} 1^+ f_2(1270) S$	0.698	0.552	<u>0.012</u>	<u>0.019</u>	0.000	0.000	0.002	0.001

Continued on next page

Table B.2 – continued from previous page

$J^{PC} M^{\epsilon}$ Isobar $L_{\xi\pi}$	$\rho(770)$		$f_2(1270)$		$f_0(1500)$		$\rho_3(1690)$	
	Δ_{m_0}	Δ_{Γ_0}	Δ_{m_0}	Δ_{Γ_0}	Δ_{m_0}	Δ_{Γ_0}	Δ_{m_0}	Δ_{Γ_0}
$2^{-+} 2^+$ $f_2(1270)$ S	0.678	0.105	<u>0.012</u>	<u>0.034</u>	0.000	0.000	0.000	0.000
$2^{-+} 0^+$ $f_2(1270)$ D	0.487	0.165	<u>0.032</u>	<u>0.009</u>	0.000	0.000	0.001	0.001
$2^{-+} 1^+$ $f_2(1270)$ D	0.366	0.154	<u>0.013</u>	<u>0.009</u>	0.000	0.000	0.003	0.001
$2^{-+} 2^+$ $f_2(1270)$ D	0.481	0.315	<u>0.002</u>	<u>0.010</u>	0.000	0.000	0.000	0.000
$2^{-+} 0^+$ $f_2(1270)$ G	0.678	0.113	<u>0.006</u>	<u>0.004</u>	0.001	0.000	0.002	0.002
$2^{-+} 0^+$ $\rho_3(1690)$ P	0.637	0.088	0.003	0.004	0.001	0.000	<u>0.001</u>	<u>0.003</u>
$2^{-+} 1^+$ $\rho_3(1690)$ P	0.800	0.299	0.005	0.008	0.001	0.000	<u>0.003</u>	<u>0.002</u>
$3^{++} 0^+$ $[\pi\pi]_S$ F	0.176	0.105	0.009	0.007	0.000	0.000	0.001	0.001
$3^{++} 1^+$ $[\pi\pi]_S$ F	0.411	0.238	0.007	0.001	0.000	0.000	0.002	0.001
$3^{++} 0^+$ $\rho(770)$ D	<u>0.246</u>	<u>0.135</u>	0.016	0.010	0.000	0.000	0.001	0.000
$3^{++} 1^+$ $\rho(770)$ D	<u>0.355</u>	<u>0.316</u>	0.006	0.004	0.001	0.001	0.002	0.001
$3^{++} 0^+$ $\rho(770)$ G	1.064	<u>0.163</u>	0.011	0.010	0.000	0.000	0.001	0.001
$3^{++} 1^+$ $\rho(770)$ G	<u>0.376</u>	<u>0.347</u>	0.004	0.006	0.000	0.000	0.002	0.001
$3^{++} 0^+$ $f_2(1270)$ P	0.589	0.029	<u>0.016</u>	<u>0.016</u>	0.000	0.000	0.001	0.001
$3^{++} 1^+$ $f_2(1270)$ P	0.279	0.190	<u>0.010</u>	<u>0.012</u>	0.000	0.000	0.001	0.001
$3^{++} 0^+$ $\rho_3(1690)$ S	0.177	0.212	0.016	0.011	0.000	0.000	<u>0.001</u>	<u>0.001</u>
$3^{++} 1^+$ $\rho_3(1690)$ S	0.151	0.263	0.005	0.001	0.000	0.001	<u>0.002</u>	<u>0.003</u>
$3^{++} 0^+$ $\rho_3(1690)$ I	0.515	0.030	0.003	0.003	0.000	0.000	<u>0.001</u>	<u>0.001</u>
$3^{-+} 1^+$ $\rho(770)$ F	<u>0.131</u>	<u>0.037</u>	0.012	0.003	0.000	0.000	0.001	0.000
$3^{-+} 1^+$ $f_2(1270)$ D	0.205	0.042	<u>0.009</u>	<u>0.003</u>	0.000	0.000	0.001	0.000
$4^{++} 1^+$ $\rho(770)$ G	<u>0.246</u>	<u>0.082</u>	0.002	0.004	0.000	0.000	0.005	0.002
$4^{++} 2^+$ $\rho(770)$ G	<u>0.252</u>	<u>0.179</u>	0.002	0.005	0.000	0.000	0.000	0.000
$4^{++} 1^+$ $f_2(1270)$ F	0.109	0.079	<u>0.003</u>	<u>0.017</u>	0.000	0.000	0.002	0.001
$4^{++} 2^+$ $f_2(1270)$ F	0.185	0.203	<u>0.001</u>	<u>0.002</u>	0.000	0.000	0.000	0.001
$4^{++} 1^+$ $\rho_3(1690)$ D	0.176	0.083	0.005	0.005	0.000	0.000	<u>0.006</u>	<u>0.002</u>
$4^{-+} 0^+$ $[\pi\pi]_S$ G	0.391	0.086	0.008	0.001	0.000	0.000	0.001	0.001
$4^{-+} 0^+$ $\rho(770)$ F	<u>0.939</u>	<u>0.309</u>	0.010	0.009	0.000	0.000	0.001	0.001
$4^{-+} 1^+$ $\rho(770)$ F	<u>0.442</u>	<u>0.294</u>	0.004	0.007	0.001	0.000	0.000	0.001
$4^{-+} 0^+$ $f_2(1270)$ D	0.881	0.166	<u>0.011</u>	<u>0.009</u>	0.001	0.000	0.001	0.002
$4^{-+} 1^+$ $f_2(1270)$ D	0.791	0.240	<u>0.002</u>	<u>0.014</u>	0.000	0.000	0.001	0.000
$4^{-+} 0^+$ $f_2(1270)$ G	0.899	0.442	<u>0.023</u>	<u>0.024</u>	0.000	0.000	0.001	0.002
$5^{++} 0^+$ $[\pi\pi]_S$ H	0.303	0.059	0.011	0.008	0.000	0.000	0.000	0.000
$5^{++} 1^+$ $[\pi\pi]_S$ H	0.473	0.142	0.006	0.004	0.000	0.000	0.001	0.000
$5^{++} 0^+$ $\rho(770)$ G	<u>0.600</u>	<u>0.191</u>	0.012	0.005	0.000	0.000	0.001	0.000
$5^{++} 0^+$ $f_2(1270)$ F	0.564	0.214	<u>0.012</u>	<u>0.019</u>	0.000	0.000	0.001	0.001
$5^{++} 1^+$ $f_2(1270)$ F	0.452	0.161	<u>0.004</u>	<u>0.004</u>	0.000	0.000	0.001	0.000

Continued on next page

Table B.2 – continued from previous page

$J^{PC} M^{\epsilon}$ Isobar $L_{\xi\pi}$	$\rho(770)$		$f_2(1270)$		$f_0(1500)$		$\rho_3(1690)$	
	Δ_{m_0}	Δ_{Γ_0}	Δ_{m_0}	Δ_{Γ_0}	Δ_{m_0}	Δ_{Γ_0}	Δ_{m_0}	Δ_{Γ_0}
$5^{++} 0^+$ $f_2(1270)$ H	0.645	0.489	<u>0.003</u>	<u>0.007</u>	0.001	0.000	0.001	0.000
$5^{++} 0^+$ $\rho_3(1690)$ D	0.271	0.278	0.010	0.003	0.000	0.000	<u>0.002</u>	<u>0.001</u>
$6^{++} 1^+$ $\rho(770)$ I	<u>0.286</u>	<u>0.091</u>	0.002	0.001	0.000	0.000	0.000	0.000
$6^{++} 1^+$ $f_2(1270)$ H	0.061	0.062	<u>0.002</u>	<u>0.005</u>	0.000	0.000	0.001	0.000
$6^{-+} 0^+$ $[\pi\pi]_S$ I	0.236	0.139	0.008	0.004	0.000	0.000	0.001	0.000
$6^{-+} 1^+$ $[\pi\pi]_S$ I	0.135	0.178	0.005	0.001	0.000	0.000	0.000	0.000
$6^{-+} 0^+$ $\rho(770)$ H	<u>0.606</u>	<u>0.046</u>	0.014	0.005	0.000	0.000	0.002	0.001
$6^{-+} 1^+$ $\rho(770)$ H	<u>0.719</u>	<u>0.136</u>	0.006	0.005	0.000	0.000	0.000	0.000
$6^{-+} 0^+$ $f_2(1270)$ G	0.477	0.074	<u>0.011</u>	<u>0.010</u>	0.000	0.000	0.001	0.001
$6^{-+} 0^+$ $\rho_3(1690)$ F	0.343	0.054	0.013	0.005	0.000	0.000	<u>0.002</u>	<u>0.001</u>
$1^{++} 1^-$ $\rho(770)$ S	<u>0.125</u>	<u>0.220</u>	0.004	0.004	0.000	0.000	0.000	0.000
$1^{-+} 0^-$ $\rho(770)$ P	<u>0.270</u>	<u>0.128</u>	0.007	0.003	0.000	0.000	0.001	0.000
$1^{-+} 1^-$ $\rho(770)$ P	<u>0.146</u>	<u>0.343</u>	0.004	0.007	0.000	0.000	0.001	0.000
$2^{++} 0^-$ $\rho(770)$ D	<u>0.171</u>	<u>0.292</u>	0.005	0.003	0.000	0.000	0.000	0.000
$2^{++} 0^-$ $f_2(1270)$ P	0.210	0.349	<u>0.011</u>	<u>0.006</u>	0.000	0.000	0.000	0.000
$2^{++} 1^-$ $f_2(1270)$ P	0.165	0.169	<u>0.006</u>	<u>0.004</u>	0.000	0.000	0.001	0.000
$2^{-+} 1^-$ $f_2(1270)$ S	0.246	0.311	<u>0.018</u>	<u>0.009</u>	0.000	0.000	0.001	0.001
Flat	0.000	0.000	0.000	0.000	0.000	0.000	0.000	0.000
Maximum	5.432	1.004	0.032	0.040	0.006	0.003	0.006	0.003

Bibliography

- [1] P. Abbon et al. »The COMPASS experiment at CERN«. *Nucl. Instrum. Meth.* A577 (2007), 455–518. DOI: 10.1016/j.nima.2007.03.026. arXiv: hep-ex/0703049 [hep-ex].
- [2] C Adolph et al. »Resonance Production and $\pi\pi$ S-wave in $\pi^- + p \rightarrow \pi^- \pi^- \pi^+ + p_{recoil}$ at 190 GeV/c«. *Phys. Rev.* D95.3 (2017), 032004. DOI: 10.1103/PhysRevD.95.032004. arXiv: 1509.00992 [hep-ex].
- [3] Jun John Sakurai. *Modern quantum mechanics*. 2nd ed. Pearson, 2010. ISBN: 0805382917.
- [4] J.D. Hansen et al. »Formalism and assumptions involved in partial-wave analysis of three-meson systems«. *Nuclear Physics B* 81.3 (1974), 403–430. DOI: 10.1016/0550-3213(74)90241-7.
- [5] David J. Herndon, Paul Söding and Roger J. Cashmore. »Generalized isobar model formalism«. *Phys. Rev. D* 11 (1975), 3165–3182. DOI: 10.1103/PhysRevD.11.3165.
- [6] C. Patrignani et al. »Review of Particle Physics«. *Chin. Phys.* C40 (2016). DOI: 10.1088/1674-1137/40/10/100001.
- [7] Frank von Hippel and C. Quigg. »Centrifugal-Barrier Effects in Resonance Partial Decay Widths, Shapes, and Production Amplitudes«. *Phys. Rev. D* 5 (1972), 624–638. DOI: 10.1103/PhysRevD.5.624.
- [8] Suh Urk Chung. *Spin formalisms*. 2nd ed. Brookhaven Nat. Lab., 2013. URL: <https://cds.cern.ch/record/1561144>.
- [9] M.E. Rose. *Elementary theory of angular momentum*. Structure of matter series. Wiley, 1957. ISBN: 0486684806.
- [10] R.A. Fisher. »On the mathematical foundations of theoretical statistics«. *Philosophical Transactions of the Royal Society of London A: Mathematical, Physical and Engineering Sciences* 222.594-604 (1922), 309–368. DOI: 10.1098/rsta.1922.0009.
- [11] George Casella, Christian P. Robert and Martin T. Wells. »Generalized Accept-Reject Sampling Schemes«. *A Festschrift for Herman Rubin*. Ed. by Anirban DasGupta. Vol. 45. Lecture Notes–Monograph Series. 2004, 342–347. DOI: 10.1214/lnms/1196285403.

- [12] Fabian Krinner. »Freed-Isobar Partial-Wave-Analyses«. Dissertation. Technische Universität München, 2018.

Acknowledgements

Three years ago, I landed alone in Europe, trying to begin a new stage of life. Now, at the time of harvest, I want to thank to people that offered me helps on the way.

Special for this thesis, I want to thank to the e18 members—I was so honored to join the group. I did my work here, talked to people, and went to group seminars. Prof. Stephan Paul, you gave me the chance for all of them. For the first time, I witnessed how people did their research, and how a large research group operated. Thank you. Dr. Boris Grube, I haven't stopped bothering you with a bunch of questions—about my work, about this thesis, about research groups and the way they do their business, even about the whole academia of physics. Well, I supposed you were really busy managing the COMPASS projects, but I always got my answers. Thank you. This thesis based on sophisticated analysis algorithm and computational techniques. Florian Kaspar offered me technical helps at departure. Also, I want to thank to all authors of the ROOTPWA program. Without this program, this thesis would not exist because none of the results can be obtained.

Of course, a three-year bachelor study consists not simply of one thesis. I still remember some important moments:

Prof. Norbert Kaiser, I was far too brave, just went to your office and asked you for a recommendation letter. I was not an impressive student, but you welcomed me warmly. Time passed, I got my letter as well as a bunch of useful advice to study and life. Thanks for your kindness. You let me know the relation between people can be simple, even if it is between a professor and a student.

Prof. Nora Brambilla, there has already been two years since I passed by a lecture hall by chance. You gave a lecture, so confidently, that I felt you were shinning. Suddenly, I felt your background resonanced with mine—foreign, female, and eager to show something of our own. My traditional Chinese shyness was hit fiercely. Since that time, I tried to keep my chin up—every time I talk to people or give a talk in front of a number of people. Thanks for reshape my character.

Dr. Oliver Dachwald and Annika, sometimes I felt I should rather be a chemist, as you weaved the fancy colors, flames and instruments in your lecture. Most

importantly, as I asked for a helium balloon as one time you used for an experiment, you promised to give me some at the last lecture. At the end, I really got them. You kept your words. I was so happy, just like the small child in the film *Life Is Beautiful* who got a real tank at the end of the story. Thank you for cherishing your promise, even not concerning the academia. You gave me a role model of the kind of people I should become.

I want to thank to the *Deutschlandstipendium*, which kept financing me since my second bachelor year. Taking part in the get-together event, I was moved from a speech given by Bianca Monzer. She said, one should always be trying to get out of his/her comfort zone to become better. Indeed, in the *Robot series* of Isaac Asimov, only the people tried to get out of the routine life in *The Caves of Steel* survived and earned the whole universe. The life of a student is far less splendid, but, the belief still often successfully prevented me from addiction to the computer games and kept me a good active state of life.

The job of a student is learning academic skills. I want to thank to the academics who gave me special offers: Dr. David Straub, Dr. Boris Grube, Prof. Stephan Paul, Prof. Stefan Schönert, Lin Han, Dr. Gabriele Witterstein, ... A working student job offer, excursions of huge laboratories, private talks about academical careers, or even a tutor position, all these chances you offered helped me know more and more about the the academia and about the possible development of myself. Thank you.

Moreover, a smooth study can not leave supports from family. Sociology told us, that quirk individuals are less acceptable to community. They face two choices for survival: Either they are strong enough on their functions. The community will acknowledge them concerning their special contributions and ignore their setbacks of the weirdness. Or they have to take painstaking efforts, cutting their edges and corners to reestablish themselves. Here, I want to thank to my father, who sponsored partly my study and passed me his strong DNA protecting me from these painstaking efforts. Weirdness also result in rebellions. The life of a rebellious girl is hard, as she has to pay for her ignorance in her latter ages. The life of the mother of a rebellious girl is even harder. Hopelessness appeared, every time the girl chose a difficult way and refused to be persuaded. I want to express my wholehearted gratitude to my mother—for every time you disagreed with but respected my choices, and kept comforting and motivating me at time I fell down paying for my choices.